1967-12

Theoretical and empirical analyses of thick skinned swept wing panels

Parcells, Paul Whitney

Monterey, California. U.S. Naval Postgraduate School

THEORETICAL AND EMPIRICAL ANALYSES OF THICK SKINNED SWEPT WING PANELS

PAUL WHITNEY PARCELLS

THEORETICAL AND EMPIRICAL ANALYSES

OF

THICK SKINNED SWEPT WING PANELS

by

Paul Whitney Parcells
Lieutenant, United States Navy
B.S., United States Naval Academy, 1960

Submitted in partial fulfillment of the
requirements for the degree of

MASTER OF SCIENCE IN AERONAUTICAL ENGINEERING

from the

NAVAL POSTGRADUATE SCHOOL
December 1967

ABSTRACT

The validity of conventional skin and stringer type analyses is verified experimentally for a thick milled skin aircraft structure. The accuracy of solution is evaluated by comparing the strain energies in a mathematical model to that obtained experimentally from a wing panel of a high performance aircraft.

Results indicate that the conventional methods of a skin-stringer/matrix force approach are valid for a thick milled skin aircraft structure of this type provided the panel loading is neither severe nor concentrated. Additionally the grid elements chosen must be small enough to preclude any gross averaging errors.

TABLE OF CONTENTS

LIST OF TABLES

LIST OF FIGURES

LIST OF PLATES

TABLE OF SYMBOLS

A	Inclosed wing cell area, square inches
a_1	Panel width (tip), inches
a_2	Panel width (root), inches
a_i	Panel end loading (tip), pounds
a_c	Panel end loading (root), pounds
AFT-IB	Aft intermediate beam
b	Panel length, inches
CIB	Center intermediate beam
E	Modulus of Elasticity, pounds per square inch
FB	Front beam
FIB	Front intermediate beam
FWD-IB	Forward intermediate beam
G	Shear modulus, pounds per square inch
l_b	Panel span (forward), inches
l_d	Panel span (aft), inches
q	Shear flow, pounds per inch
RB	Rear beam
RIB	Rear intermediate beam
T	Torque, inch pounds
t_t	Panel thickness (tip), inches
t_r	Panel thickness (root), inches
U	Internal strain energy, inch pounds
V	Constant voltage source, volts
V_o	Wheatstone Bridge output voltage, volts

w_i	Panel edge length, inches
w_c	Panel edge length, inches
x_w	x-axis co-ordinate of wing, inches
y_w	y-axis co-ordinate of wing, inches
β	Panel angle (AFT-IB to pivot rib), degrees
δ	Panel angle (RIB to intermediate rib), degrees
μ	Poisson's ratio
ϵ	Strain, micro-inches per inch
σ	Normal stresses, pounds per square inch
τ	Shear stresses, pounds per square inch
θ	Angle of twist per unit length, radians per inch
ϕ_p	Angle of principal axis measured from the first gage of the rosette, degrees

CHAPTER I

INTRODUCTION

Aircraft structures in general, and wings in particular, have been constructed using the conventional stringer and sheet methods. This form of construction, by nature not a simple structure, introduced the problem of how to accurately predict the load distribution and especially the stress concentrations that could be developed. The oldest representation scheme for the discrete element analysis of the problem evolved as the axial force member-shear panel idealization that is described in Reference 1. This method is particularly acceptable to the aircraft industry, as it readily lends itself to various matrix techniques that are easily adaptable to a digital computer for solution. Generally speaking, this method of solution makes no provision for accounting for Poisson's ratio and sweep effects.

With the advent of the very heavy milled skins of modern high performance aircraft, one immediately questions the validity of the conventional form of solution. In order to properly account for bending-torsion interaction, chordwise curvatures, sweep coupling, shear deflections, and the increasing use of large cutouts, several alternative methods of analysis have been developed.

The most widely used solution technique is outlined by J. H. Argyris and S. Kelsey in Reference 2. The aircraft structure is molded into a large assemblage of elastic elements, which permits matrix formulation of the solution in

terms of the different energy theorems. The fundamental principles originated by Maxwell and Mohr of virtual forces and virtual displacements are used in the energy method of solution. A practical application of this technique is included in References 3 and 4.

The objective of this study is to determine the validity of this lumped parameter form of a theoretical analysis for thick skinned structures. Because of the general energy approach to the solution, the method chosen to determine the accuracy of the results was to compare the total internal strain energy of an idealized panel with that of an actual thick milled skin aircraft structure of the same dimensions. The structure would have to be thick enough to be able to support any bending-torsion interaction that may exist in addition to the inplane loadings.

The objective of this report was to be achieved by comparing the theoretical strain energy of a structure with that determined empirically from strain gage readings. The structural specimen to be analyzed was a single wing panel taken from the port wing upper skin of a Mach 2.5 all-weather fighter project which was canceled by the U. S. Navy before the structural test program was completed.

The necessary strain gage rosettes and accompanying instrumentation were installed, and a comparison of the theoretical and empirical analyses was made.

A literature search did not reveal any reference that made a comparison of the energy level in an idealized

structure to that of an actual wing panel element. The importance of a comparison of this type is apparent when one realizes that the integrated behavior of a structure is dependent upon the energy accounting in the system.

This study was completed during the 1967-1968 academic year at the Naval Postgraduate School, Monterey, California. Acknowledgement is gratefully made to Professor C. H. Kahr of the Aeronautics Department for his guidance and consultation as thesis advisor; R. A. Besel and T. B. Dunton, laboratory technicians; and CAPT D. B. Messerschmidt, USMC who, while working on a similar thesis project, aided in this study.

CHAPTER II

THEORETICAL ANALYSIS

The structure chosen for study was the wing center section of an F8U-3 type aircraft. The particular panel analyzed was the port section bounded longitudinally by the pivot and intermediate ribs and laterally by the aft-intermediate and rear-intermediate beams. The wing center section and specific panel are graphically depicted in Figure 1.

The typical industrial approach to analyzing a structure of this nature would be to determine what valid simplifying assumptions could be made in order to create a mathematically simple idealized structure. The resulting model would consist of axial load carrying bars and plane shear carrying constant thickness panels. The idealized model was developed and is thoroughly discussed in References 3 and 4.

The load application was accomplished by applying a torsional moment at the wing fold rib, about the load reference axis (CIB). Considering the port wing inboard of the intermediate rib, this couple must be distributed, using elementary torque theory, to the equivalent loads on a streamwise cross-section (intermediate rib) at station $y_w = 81.98$ (Figure 2). The loading was then divided among the six cells of the wing. The shear flow for each cell was determined in accordance with Reference 1 by equating

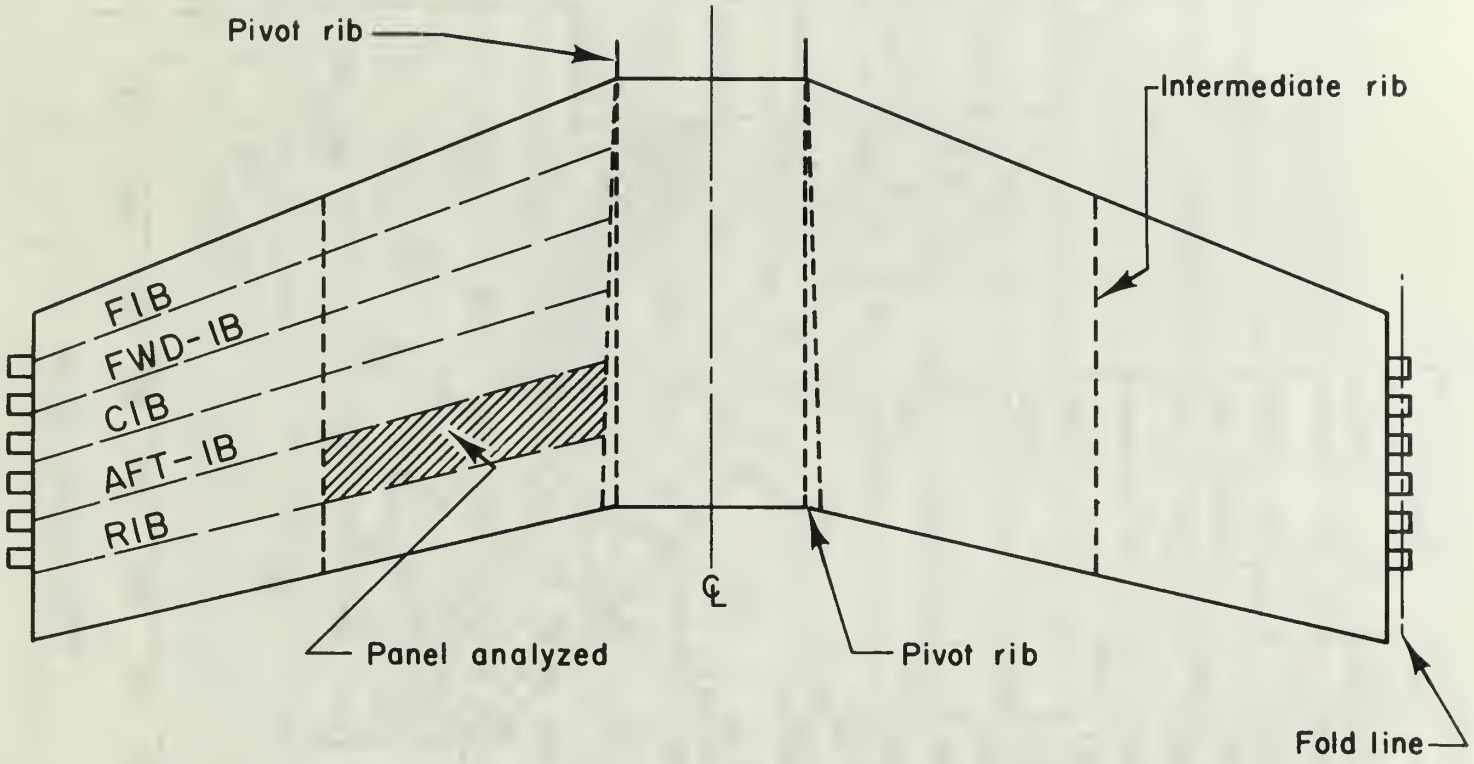

FIG. 1

SKETCH OF F8U-3 WING CENTER SECTION

FIG. 2
CENTER SECTION - F8U-3, PORT WING
(Main structural elements)

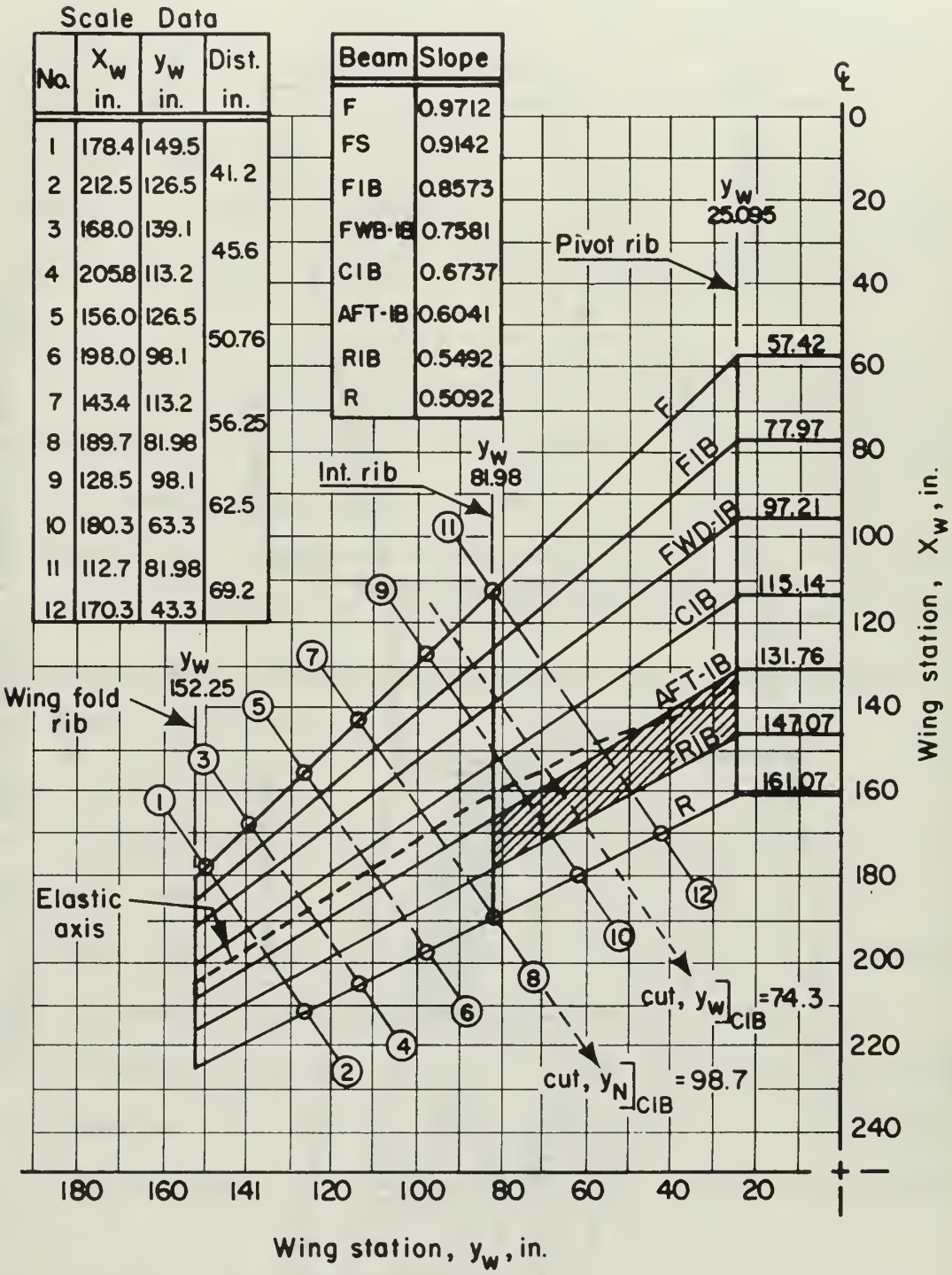

the angle of twist of one cell with the remaining five and equating torsional moments as follows:

$$T = \sum_{1}^{6} 2Aq \qquad (1)$$

The results and calculations of the shear flows were calculated in Reference 3 and are included in this report as Appendix A with inappropriate sections deleted. Using the planform dimensions of Figure 2, the shear flow for each cell was determined as oriented perpendicular to the CIB.

Figure 3 shows the idealized panel section of the wing with pertinent dimensions obtained from Reference 5. The internal strain energy of this skewed shear panel was calculated in accordance with S. J. Garvey (Reference 6) as follows:

"Since by similar triangles, the perpendicular distance of any point in a trapezoidal panel to a parallel edge is proportional to the depth of the panel at that point measured parallel with a side, the well-known result follows that the "shear flow" in a trapezoidal panel is inversely proportional to the square of the depth."[6]

To find the strain energy, using these geometric simplifications of a trapezoid, one must solve the following equation:

$$U = \frac{q_4^2}{2Gt^2}\left\{1 + \frac{2}{3(1+\mu)}\gamma\right\} \times \text{Volume} \qquad (2)$$

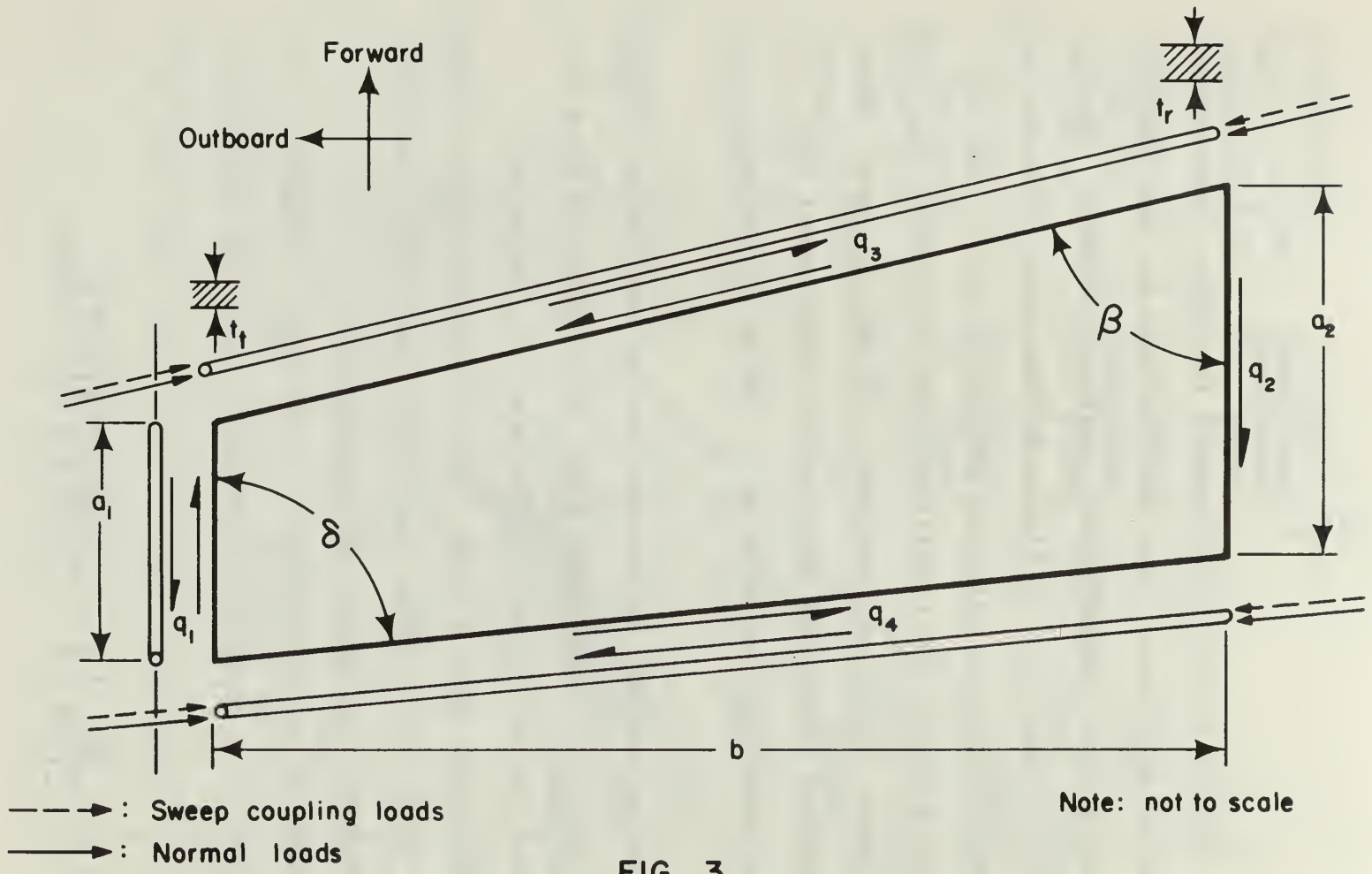

FIG. 3
IDEALIZED PANEL ON F8U-3, PORT WING

where:

$$\gamma = \cot^2\beta + \cot\beta \cot\delta + \cot^2\delta \tag{3}$$

Table I lists the appropriate dimensions and constants needed for the theoretical analysis. The volume of the plate was determined for the idealized panel from:

$$V = \left(\frac{a_1 + a_2}{2}\right) b \left(\frac{t_r + t_t}{2}\right) \tag{4}$$

This approach of utilizing the average thickness will obviously limit the accuracy of the resulting theoretical strain energy; however, the objective of this part of the analysis is to obtain the strain energy by the same conventional methods currently being used by industry.

As previously discussed, the plate edge loadings were determined from a linear interpolation using the planform dimensions. These shear panel edge loadings were distributed around the perimeter of the panel, in accordance with Reference 4, by first assigning a unit shear force to the outer edge of each panel. Considering a typical panel as shown in Figure 4 and taking moments about appropriate points to ensure the maintenance of equilibrium, the following ratios of edge forces were derived:

$$a_b = a_i \frac{l_b}{w_c} \tag{5}$$

TABLE I

PANEL PARAMETERS

Parameter	Value	Units	Reference
μ	0.32		7079-T6 Al
G	3.9×10^6	psi.	7079-T6 Al
E	10.3×10^6	psi.	7079-T6 Al
a_1	12.132	in.	Ref. 5
a_2	15.247	in.	Ref. 5
b	56.885	in.	Ref. 5
t_r	0.62	in.	Ref. 5
t_t	0.33	in.	Ref. 5
t_{ave}	0.477	in.	- - -
δ	61^o 13'	deg.	Ref. 5
β	58^o 52'	deg.	Ref. 5

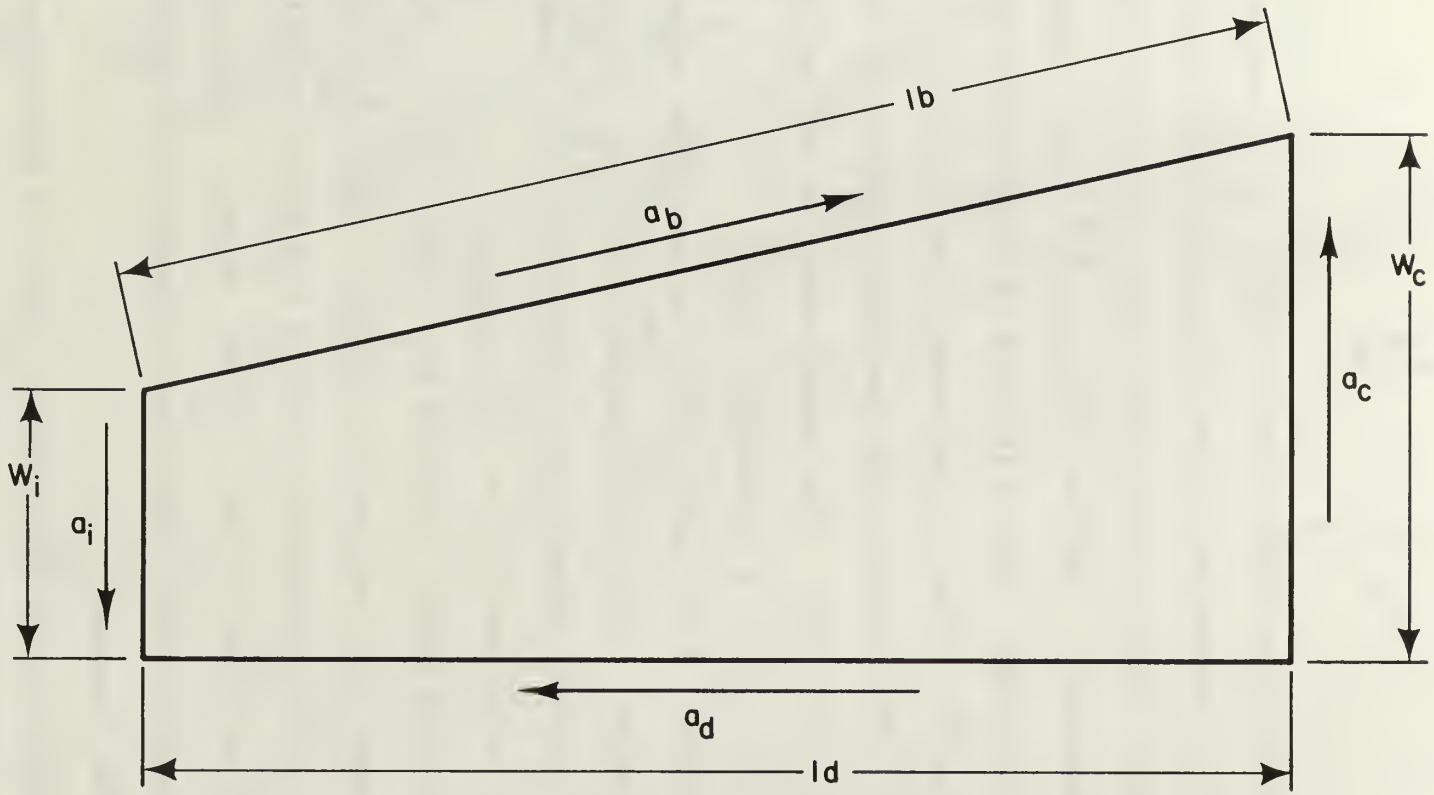

FIG. 4

TYPICAL PANEL SHOWING DIMENSIONS FOR EDGE LOADING RATIOS.

$$a_c = a_i \frac{W_i}{W_c} \tag{6}$$

$$a_d = a_i \frac{l_d}{W_c} \tag{7}$$

The Matrix Force Method is described in Reference 11 and was used to determine the end edge loadings on the panels. These loads were obtained from previous calculations in Reference 3. The end edge load for the particular panel studied in this report (Figure 5) was then scaled to the edge utilized in the strain energy calculation of Equation (2). This scaled load was then divided by the length of the same edge. The result was the desired edge shear flow (q_4 = 325.976 pounds per inch).

Substitution of the appropriate values from Table I and the computed shear flow into Equations (2), (3), and (4) will yield the total shear panel internal strain energy. The resulting value was 33.280 inch pounds.

The idealized model, being a pure shear panel, was incapable of supporting any axial loadings. For this reason the effective cross sectional area of the plate was divided evenly and distributed to the adjacent flanges (Figures 3 and 5). The axial loads were then assumed to be applied directly to the flanges.

In accordance with Reference 9, sets of additional axial forces (dashed forces in Figures 3 and 5) were applied to the ends of the flanges. The forces are necessary to

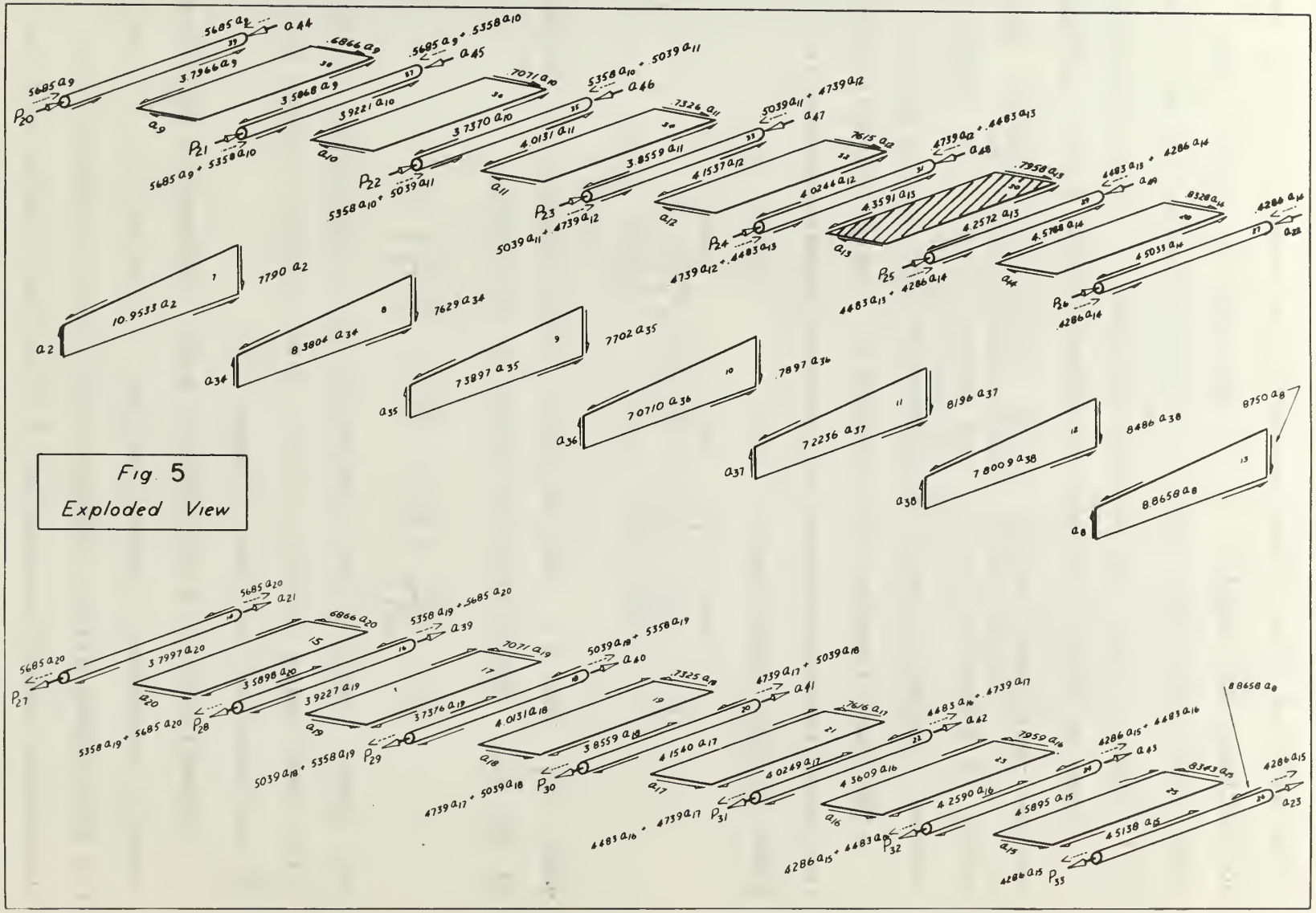

Fig. 5
Exploded View

account for the additional strain energy stored by the axial components of shear flows caused by the sweep effect of the non-rectangular panels. It is important to realize that these sweep coupling loads are internal forces and would not be included in the equilibrium equations of the structure.

From an energy standpoint, these dashed forces account for the additional strain energy stored in the panel. The energy is accounted for in this manner because the longitudinal flanges contain the effective area of the panel.

The contribution of a uniform bar under linearly varying axial forces to the total internal strain energy is given in Reference 9 as,

$$U = \frac{1}{2AE} \int_0^{\ell} \left(P_i + \frac{P_i - P_j}{\ell} x \right)^2 dx \tag{8}$$

where P_i and P_j are the axial forces applied to the ends of the bar. Integration of Equation (8) yields:

$$U = \frac{\ell}{6AE} \left(P_i^2 + P_j^2 + P_i P_j \right) \tag{9}$$

The flange loadings were determined as a percentage of the total load based on the ratio of the effective flange area of the panel to the total flange area.

Substitution of appropriate panel parameters and previously determined flange loadings into Equation (9) yields the additional strain energies required to complete the theoretical energy accounting.[3] The distribution of the energies is listed in Table II.

TABLE II

THEORETICAL STRAIN ENERGY DISTRIBUTION OF THE IDEALIZED MODEL		
Shear Panel	33.280	inch pounds
Forward Flange	0.313	inch pounds
Rear Flange	1.067	inch pounds
Rib Flange	0.046	inch pounds
TOTAL ENERGY	34.706	inch pounds

CHAPTER III

DISCUSSION OF THEORETICAL RESULTS

The concept of the idealization, as discussed in Reference 11, is simply to assign all the direct stress carrying capacity of the structural material to the axial force members and the shear carrying capacity to the shear panel.

The idealization yields a theoretical solution to the problem that utilizes several different averaging processes; however, the objective of this report is to analyze the accepted conventional methods currently in use in the aircraft industry.

The distribution of the panel area to the adjacent flanges is complicated by the apparent double use of the area near the tip of the panel. Several wing analyses have described alternative methods of including the rib flange in the idealized structure.[12] It is of interest to note that the theoretical result of the strain energy determined for the rib flange is insignificant when compared to the other components of the strain energy in the structure. Because of the small energy of the rib flange portion of the plate contribution, one could conclude that this flange and similar pieces do not contribute significantly to the over-all wing behavior. Therefore, as discussed in Reference 12, analyses of wings with applied normal loadings could be simplified considerably by assuming zero flexibility for this flange. It should be noted that the application of

chordwise loads would require that these elements be included. This approach would appreciably decrease the number of redundants in a wing analysis.

An appropriate study might be the determination of the contribution of these rib flanges to the integrated analysis of the wing.

CHAPTER IV

EXPERIMENTAL ANALYSIS

In order to determine the actual strain energy and compare it with the value predicted from theory, an experimental investigation was completed on a panel of an F8U-3 wing acquired from the Ling-Temco-Vought Corporation. The panel section was a typical thick milled skin portion of the wing and was tapered along the span as well as in the chordwise direction.

The detailed explanation of the wing installation and loading is included in Reference 3; therefore, only the highlights of installation and any modifications incorporated by the author will be included in this report.

The wing was mounted inverted on a rigid support jig. It was fastened to the jig at the two fuselage pivot lugs and the two points on the main box front beam directly opposite the bumper points (Plate 1). Aluminum pads were installed under the jig to distribute the loading to the laboratory floor.

The entire wing was subjected to two pure torque loads applied at each wing fold rib about the CIB (Plate 2). The position of the elastic axis was obtained from manufacturer's data and is shown in Figure 2. The CIB is approximately parallel to the elastic axis in the outboard section of the wing. It reflects the characteristic breakdown in the concept of a load axis toward the root of a swept wing.

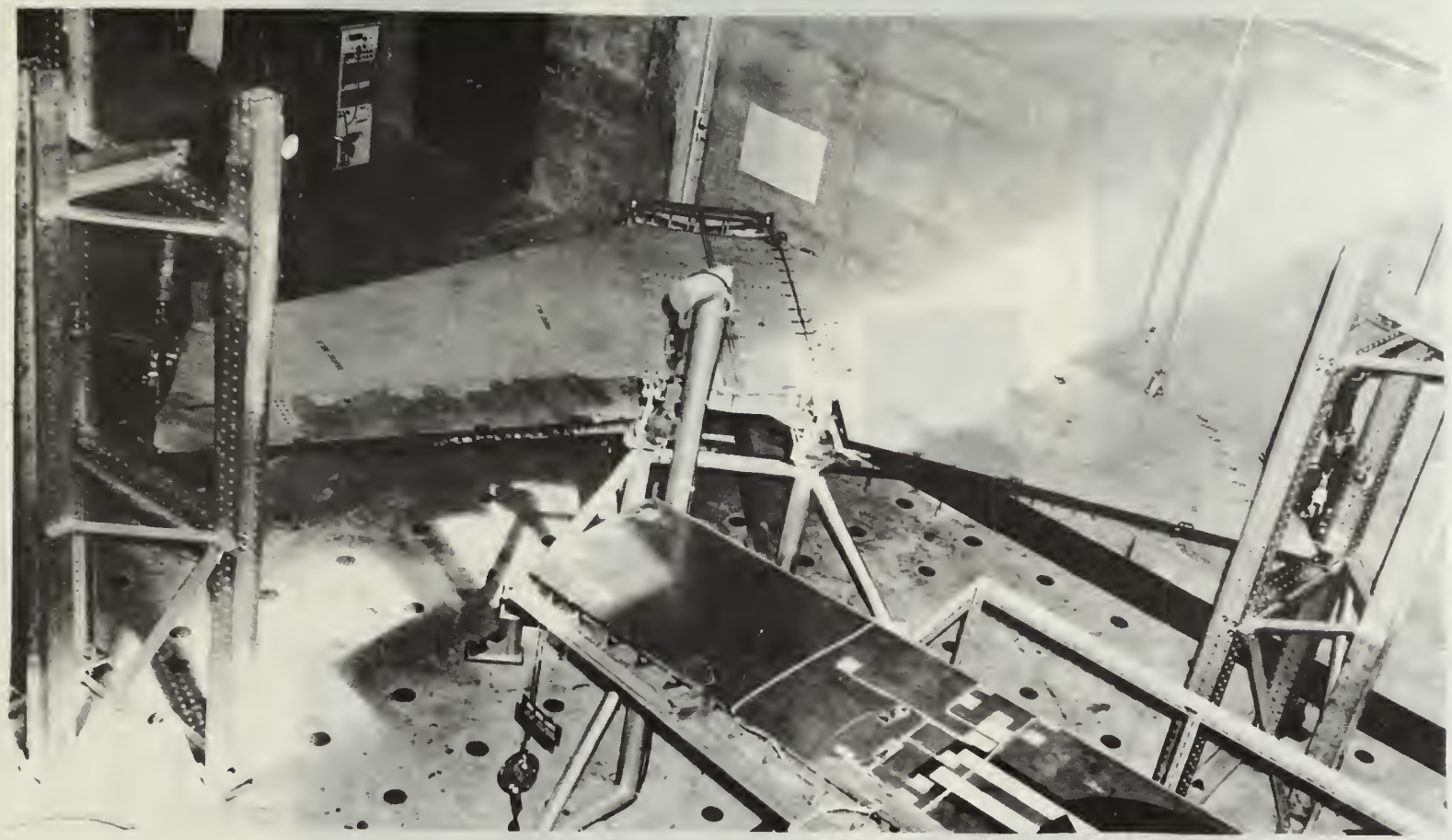

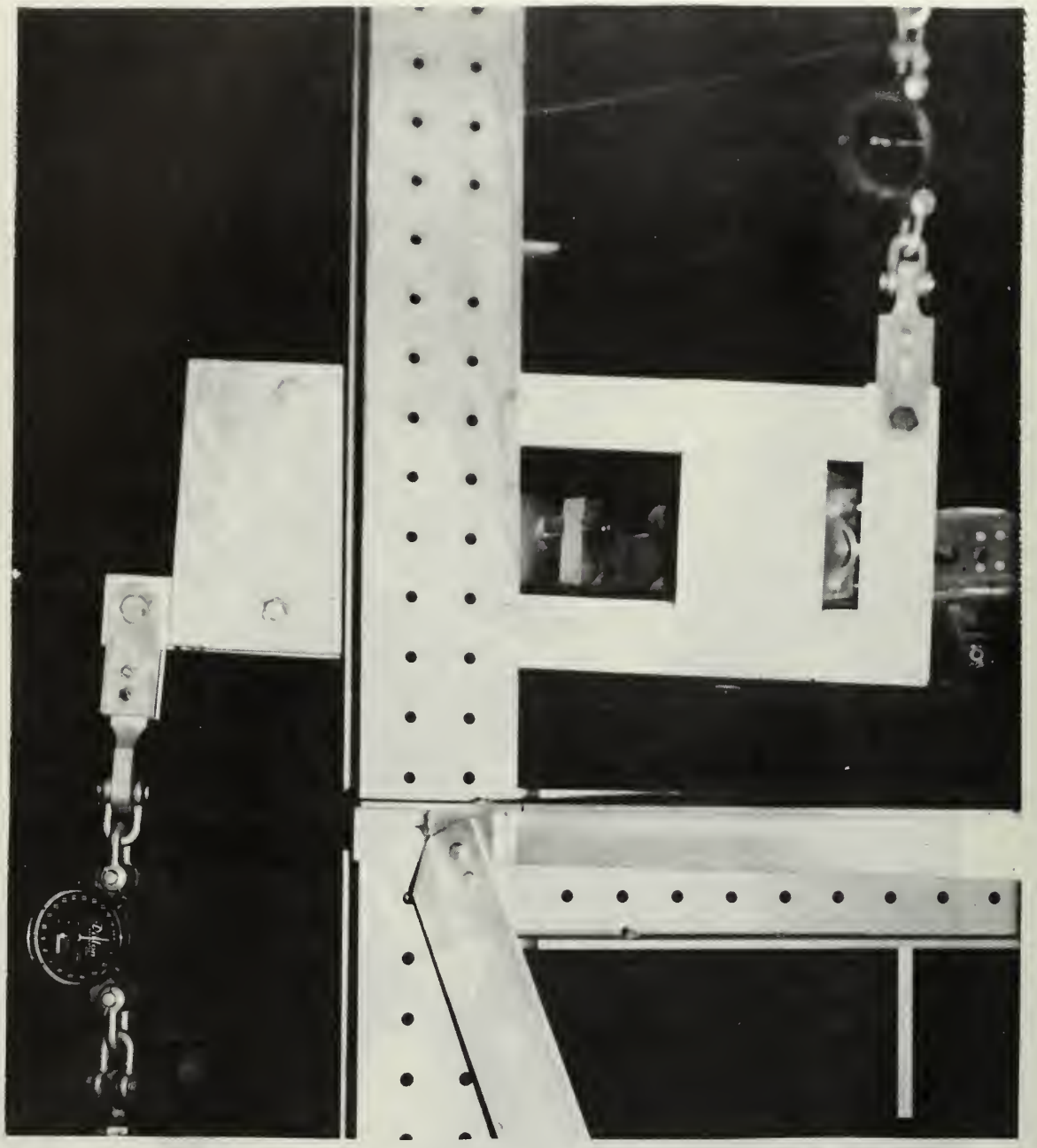

PLATE 2

PITCH MOUNTING FOR ECM ILLUMINATOR

The predetermined loading (8,000 pounds or 336,000 inch pounds of torque) was measured with 10,000 pound dynamometers connected in series with each hydraulic loading cylinder. They were graduated in 100 pound increments but could be read accurately to ten pounds. The final load magnitudes were determined with hydraulic manifold pressure readings related to pressure-load calibration curves for the cylinders found in Appendix B. The load was well within the elastic limit of the wing structure but still of sufficient magnitude to yield adequate strain levels throughout the structure.

All outer surface strain gage installations on the test panel were installed by the author. The internal gages were installed by laboratory technicians. All strains were measured with SR-4 strain gage rosettes of the type AR-7-2 manufactured by the Baldwin-Lima-Hamilton Corporation. Appendix C is a list of all 102 gages, their gage factors, resistances and co-ordinate locations on the panel. The rosettes on the outer surface were installed back to back with the inner gages in order to give an indication of any differential bending effects through the thickness of the panel that may have existed. Figures 6 and 7 graphically depict the strain gage locations on the panel, and Plate 3 shows the interior gage installation. A twenty channel Budd Company switching and balancing unit was connected to an externally powered Wheatstone bridge circuit. The bridge and all associated circuitry were an integral part of a

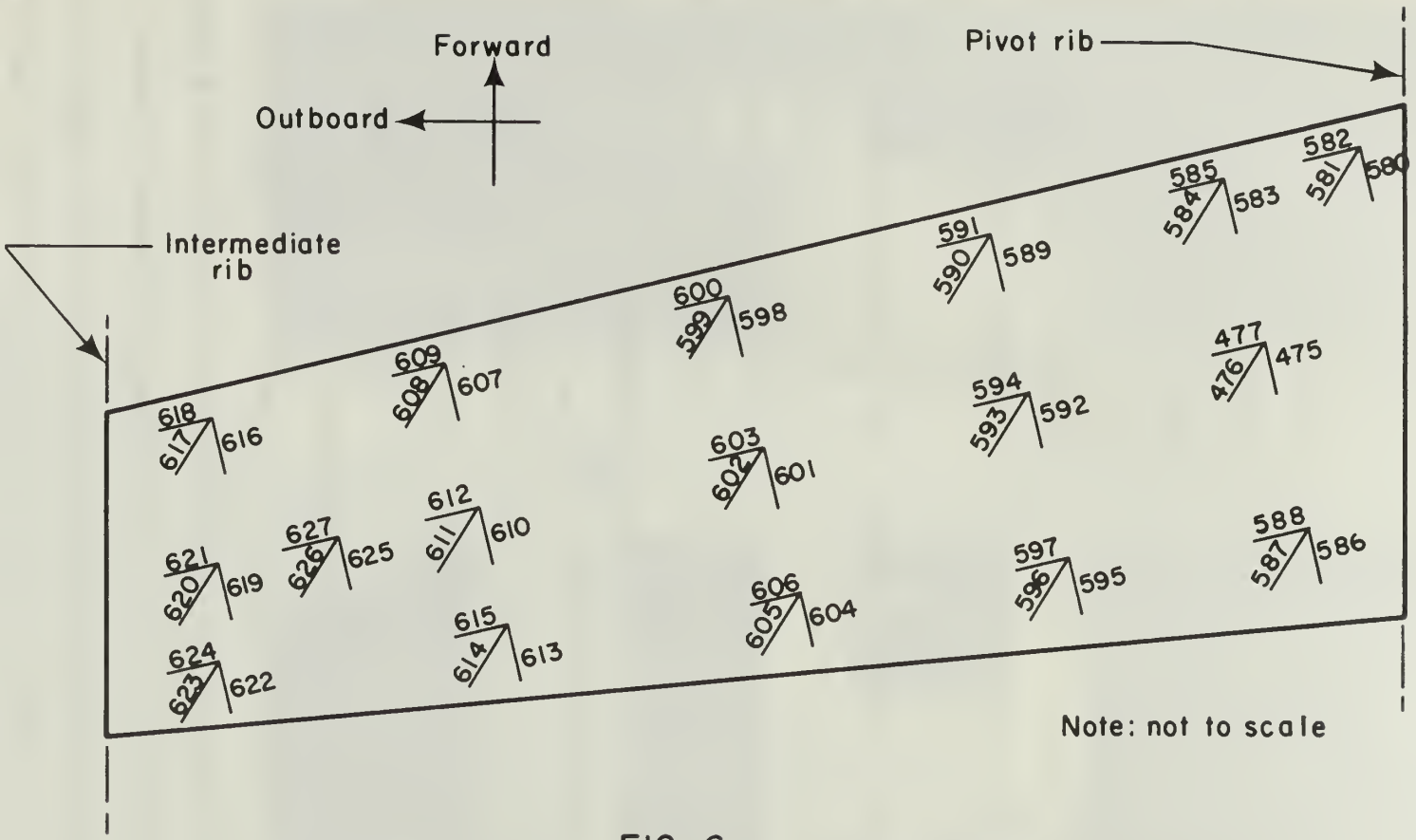

FIG. 6
SKETCH OF STRAIN GAGE LOCATIONS
(Outer-skin)

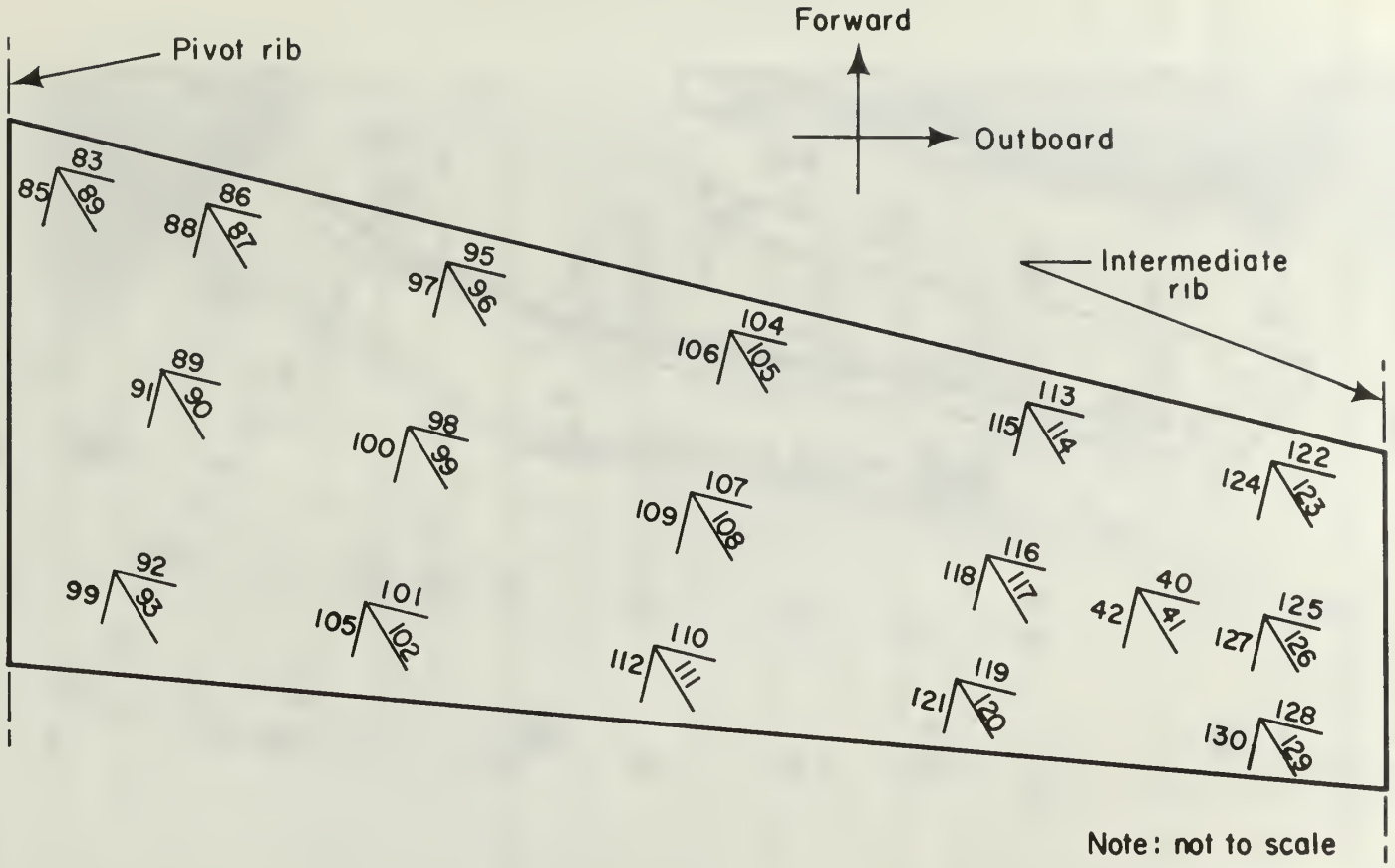

FIG. 7
SKETCH OF STRAIN GAGE LOCATIONS
(Inner - skin)


TEST PANEL

Budd/Datran Digital Strain Indicator (Model TC22) that read out strain directly in micro-inches per inch. Calibration of all equipment preceded each run. The electronic set-up is described in Reference 3 and is reproduced in this report as Appendix D.

The procedures used in conducting all test runs were as follows:

1. The digital indicator was calibrated before each run ensuring that sufficient time was taken between runs to preclude any errors being induced from hysteresis effects.
2. The switching and balancing unit leads were plugged into twenty gage terminals at the junction panel (Plate 4).
3. All strain gages and dynamometers were zeroed.
4. The hydraulic torque loading was applied and adjusted to agree with all previous runs.
5. Equal couple loadings applied to each wing tip were ensured by comparing the dynamometer readings.
6. The strain readings were taken and recorded.
7. The loads were removed. Hysteresis effects were removed by allowing sufficient time (8 to 10 minutes) before commencing the next run.

Because of ambient laboratory temperature changes, the sun striking the wing, and outside electrical interference, all test runs were conducted at night. To ensure steady

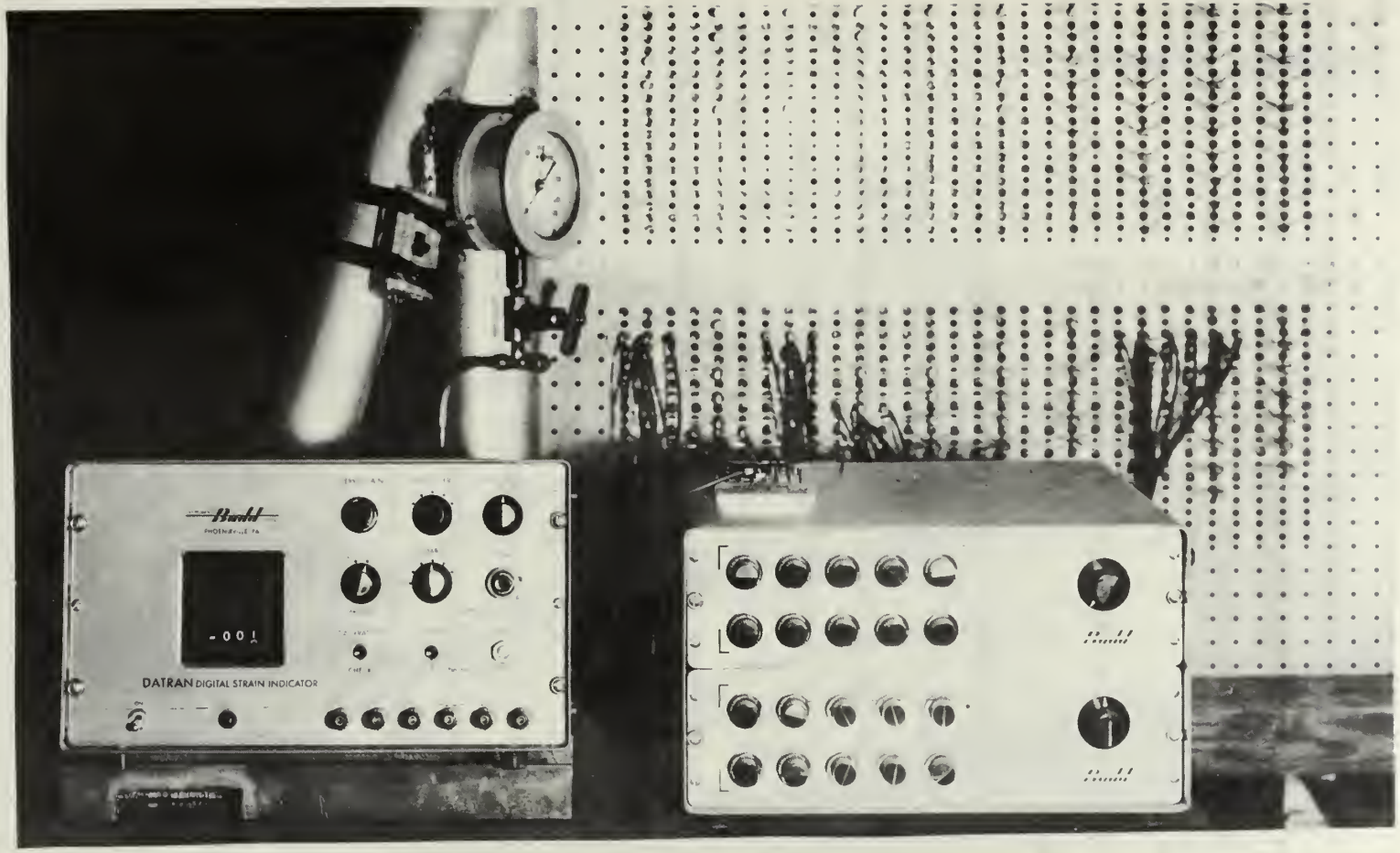

PLATE A

EQUIPMENT INSTALLATION

state conditions an adequate (approximately one half hour) warm-up time was used for all associated equipment. Repeatability of strain gage readings was ensured by check runs being made periodically and compared with those previously obtained. The percentage difference in readings was minute and was considered to have an insignificant effect on the analysis.

As stated earlier, the objective of the experimental phase of this analysis was to correlate the theoretical results that were previously obtained; therefore, once the recorded strain data were obtained, the experimental total strain energy in the plate was to be determined. Reference 7 discusses the calculation of strain energy in a structure in a general form that is applicable to the panel considered in this report. The general form of the total strain energy is given by,

$$U = \iiint_V \left[\frac{1}{2E}\left(\sigma_x^2 + \sigma_y^2 + \sigma_z^2\right) - \frac{\mu}{E}\left(\sigma_x\sigma_y + \sigma_y\sigma_z + \sigma_z\sigma_x\right) + \frac{1}{2G}\left(\tau_{xy}^2 + \tau_{yz}^2 + \tau_{zx}^2\right)\right] dx\, dy\, dz \tag{10}$$

In the wing panel of this report, where σ_z, τ_{yz}, and τ_{zx} are all nearly zero for plates/panels of this type, the stress condition indicated by Equation (10) reduces to the following:

$$U = \frac{1}{2}\iiint_V \left[\frac{1}{E}\left(\sigma_x^2 + \sigma_y^2 - 2\mu\sigma_x\sigma_y\right) + \frac{1}{G}\tau_{xy}^2\right] dx\, dy\, dz \tag{11}$$

This strain energy formula of the stress state in Cartesian co-ordinates is the same as that related by A. D. M. Grzedzielski in Reference 8. Here the terms have the following meanings: τ_{xy}^2 term represents the shear energy of the panel. The σ_x^2 and σ_y^2 terms reflect the inplane and bending/torsion energies. The term containing $\sigma_x \sigma_y$ introduces the Poisson's ratio coupling.

Strain gage data were programmed into an IBM System/360 Model 67 digital computer to obtain the principal stresses and directions at all rosette locations. A FORTRAN IV program "RECROSE" was written to convert the strain readings to the desired stresses. The discussion of the computer program and the results are included in this report as Appendix E.

The test panel was then partitioned into fifteen sub-panel elements. The partitioning of the panel (Figure 8) would permit a summation of strain energies over the panel that would yield the total strain energy. This process is a close approximation to the integration required in Equation (11). The strain readings were averaged where more than one gage existed. Both the inside and outside rosettes on each sub-panel were included. The results of the sub-panel averaging are listed in Table III. The sub-panel thicknesses used to compute the volumes were the average sub-panel thicknesses obtained from Reference 10. A graph of the panel thickness versus y_w is included in this report as Figure 9.

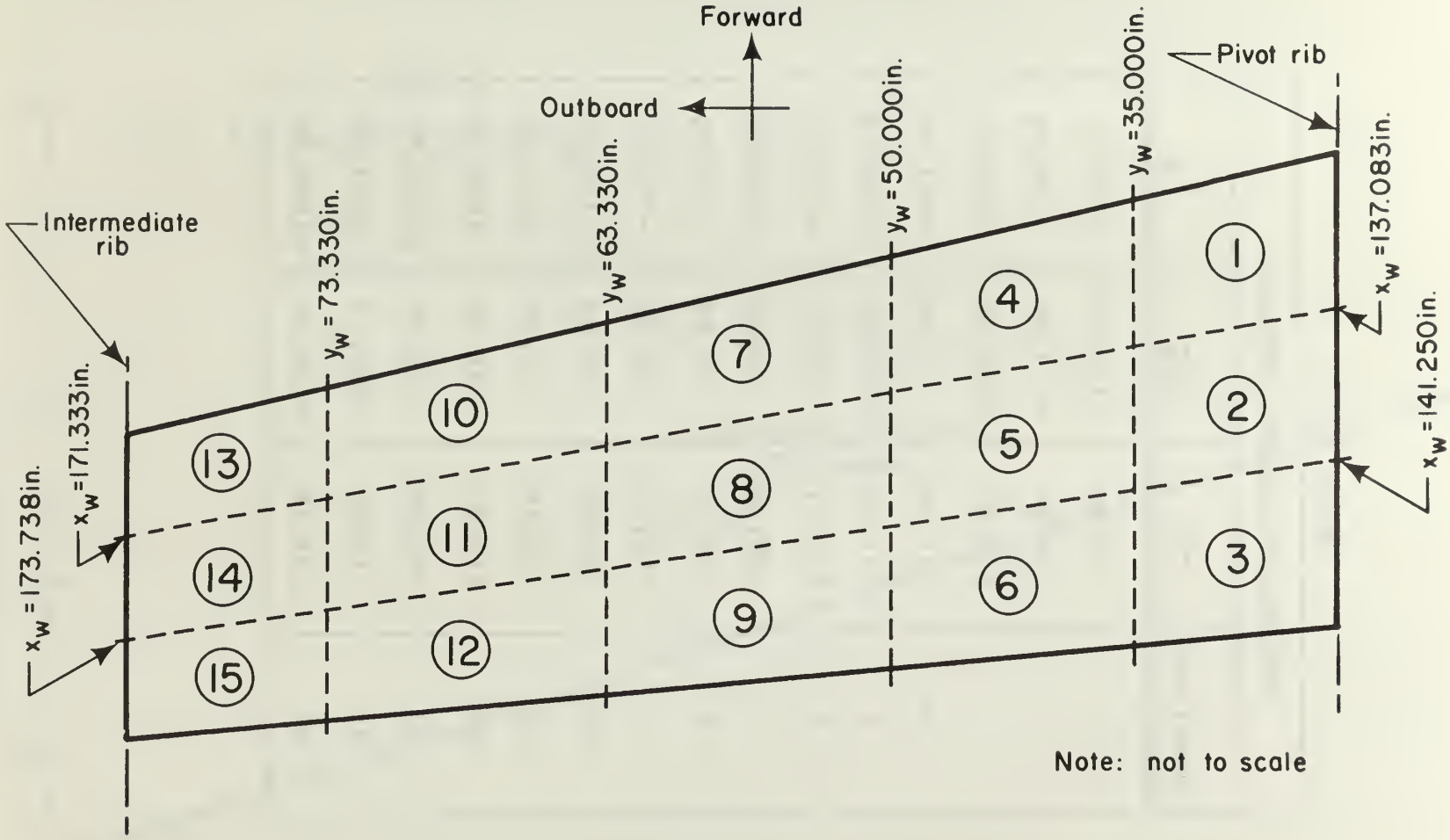

FIG. 8
SKETCH OF PLANFORM OF PARTITIONED PANEL

TABLE III

AVERAGE SUB-PANEL STRESSES			
Panel No.	σ_1	σ_3	τ_{13}
1	76.94	-115.93	-490.25
2	119.37	-173.96	-338.28
3	141.58	-203.99	-502.31
4	157.43	-71.62	-661.05
5	237.09	-104.48	-669.08
6	215.11	-90.22	-691.19
7	188.63	-40.42	-898.64
8	165.23	-63.82	-910.20
9	244.65	-80.84	-870.01
10	153.65	-83.44	-1139.25
11	220.78	-72.57	-1127.20
12	218.42	-46.80	-1064.91
13	250.56	-78.95	-1225.65
14	174.92	-182.72	-1291.96
15	231.18	-106.37	-1285.93

FIG. 9

SKIN THICKNESS VARIATION WITH SPAN.

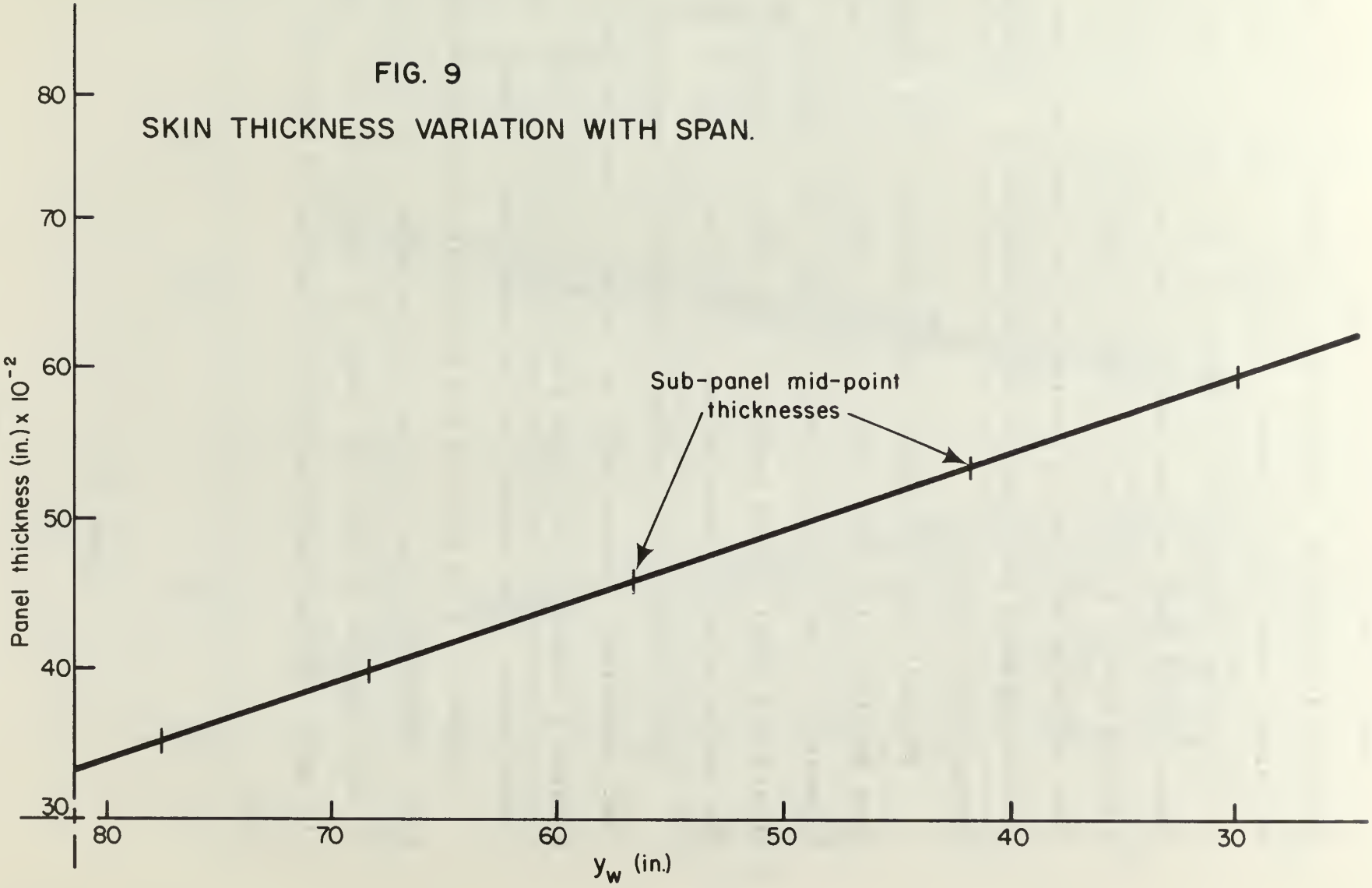

The differences between the inner and outer surface stresses (Appendix E) indicate that a bending/torsion effect definitely does exist; however, assuming a linear variation of the stress through the thickness of the plate produces a strain energy that is less than one per cent different from a direct stress averaging technique. Therefore, the mid-plane stresses obtained by averaging the inner and outer surface stresses were used in the calculation of the experimental strain energies.

The individual sub-panel strain energies were computed from Equation (11) using the required stresses listed in Appendix E. The sub-panel energies were then summed to obtain the total strain energy of the entire wing panel. The result of this summation was 33.714 inch pounds.

The internal strain energy thus obtained was nearly that determined theoretically in Chapter II and was considered a reasonably accurate evaluation of the actual strain energy that existed in the swept panel element.

Figure 10 is a plot of the principal stresses obtained from "RECROSE" versus location on the panel. The purpose of this graph is to give the reader a feeling for the overall panel loading under the applied loading of the whole wing.

FIG. 10

EXPERIMENTAL PRINCIPAL STRESSES

(Averaged along streamwise chord)

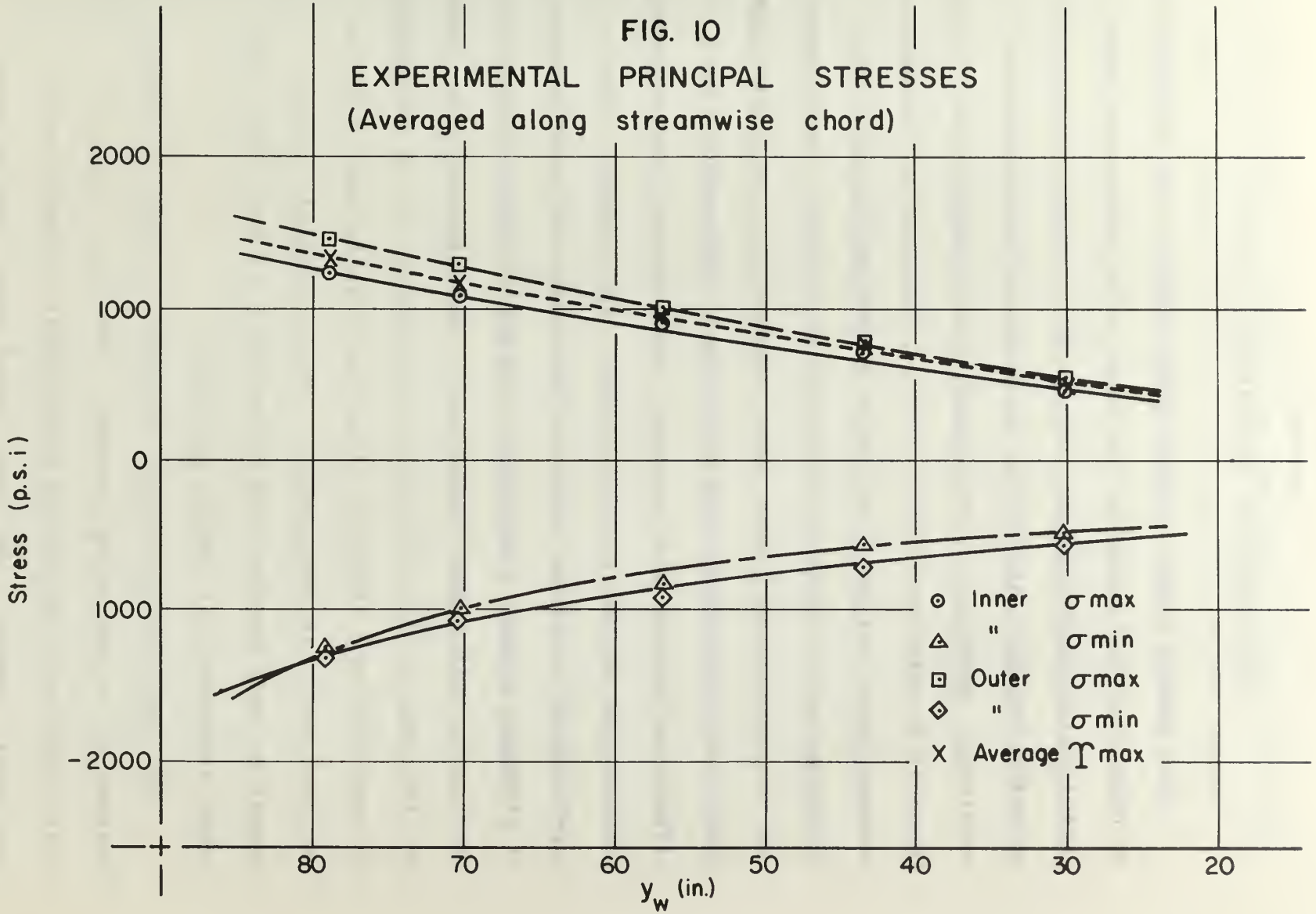

CHAPTER V

DISCUSSION OF EXPERIMENTAL RESULTS

The strain gages on the outer surface were mounted back to back with the interior rosettes. The purpose of this installation was to detect any bending present that would be reflected in a difference in inner and outer strain readings. Examination of Figure 10 and Table E4 in Appendix E indicates that bending definitely does exist. However, when a linear variation of stress through the thickness of the plate is assumed, the strain energy does not vary appreciably from that computed by direct averaging; therefore, even though the wing panel does exhibit the effects of bending and twisting, the internal strain energy computations do not seem to reflect this effect. The experimental analysis averages the inner and outer values of stresses before determining the panel strain energy; therefore, this method utilizes the midplane stresses that are the mean of the two surface stresses. It is significant to note that the stresses along the rosette legs must be utilized for this computation. The principal stresses cannot be used because the orientation of the inner and outer stresses will not be parallel.

The experimental result obtained utilizes different degrees of an averaging process. Obviously, this will not yield precisely the strain energy that actually exists in the panel; however, the partitioned panel strain energy

that was computed by summing the sub-panel energies must be as close as possible to the actual internal strain energy that exists. The further partitioning of the panel into smaller elements would require the installation of more strain gage rosettes. This would possibly further improve upon the accuracy of the experimental strain energy results; however, this approach was precluded by both time and monetary considerations.

The optimum installation of the strain gage rosettes would have been to place them in the center of each of the fifteen sub-panel elements; however, the internal gages having been previously mounted and the desirability of mounting the inner and outer gages back to back precluded the optimum installation. Additionally, because of the lack of any stress concentrations, the stresses did not vary radically over the panel. For these reasons the rosette installations were considered adequate for this analysis.

CHAPTER VI

COMPARISON OF RESULTS

The comparison of the theoretical and experimental results, obviously, in the final analysis depends on how well the energy of the mathematical model approximates the true energy of the system. As stated in Reference 8, one should not expect a correct result from either a mathematical model or a lumped averaging process similar to the empirical approach taken in this report unless the load distribution is uniform over the panel. The strain energy error becomes smaller if a more finely partitioned grid is used. Thus, when the panel is subdivided into smaller elements, the lumped integral form of computing strain energy will increase in accuracy.

The error occurring in the determination of the theoretical strain energy is obtained from the following:

$$\frac{U_e - U_t}{U_e} = \text{percentage error} \tag{12}$$

Utilizing the results obtained in these analyses, the percentage error in the theoretical strain energy computation was found to be 2.94 per cent.

It appears that there have been no gross errors made in the energy accounting procedures. The comparison made indicates a remarkably close agreement between experimental and theoretical results.

Superficially, one might expect the experimental strain energy to be greater than that computed from the idealized model. This would seem reasonable when one considers that the theoretical solution for a shear panel cannot possibly include the strain energies induced from bending, torsion, and any cross coupling effects that may exist in the actual thick milled skin panel; however, careful scrutiny of the idealized model reveals that the Poisson's effect is not included; and therefore, there is no mechanism to include the chordwise stresses. In fact, they are neglected. On the other hand, in the empirical analysis it is shown that appreciable chordwise stresses do exist. This is a contradiction to the close agreement (2.94 per cent) in the comparison of the strain energies.

From this discussion one must conclude that the stresses determined theoretically in Reference 3 must have been in excess of their true values. This excess of spanwise and shear stresses would compensate for the lack of chordwise stresses. This is the only logical explanation for the close comparison of the two analyses.

In order to determine the validity of this reasoning, the principal stresses at station Y_w = 34.50 inches were compared. The stresses in the model were: σ_{max} = 714 psi and τ_{max} = 596 psi. Similarly, the experimental stresses obtained from Figure 10 were: σ_{max} = 525 psi and τ_{max} = 517 psi.

As was predicted, the idealized normal stresses were considerably higher (26.30 per cent) than those obtained empirically. Similarly, the theoretical shear stresses were higher (13.25 per cent). In general, these overestimates of stress values compensated for the lack of chordwise stresses when the theoretical strain energy was computed.

The location of the test panel on the wing did not lend itself to the direct application of severe bending and/or torsional loads. One can conclude, therefore, from the results of this report that when even thick skinned aircraft structures are analyzed using the conventional lumped stringer and shear panel method, the analysis will be valid provided there are no severe bending or torsion loads applied directly to the panel. In general, the conventional method is valid, provided that the structure is sufficiently partitioned into a fine enough grid structure and the load distribution is not too irregular.

In conclusion, one should not expect from an analysis based on the lumped stringer and shear panel concept a satisfactory agreement with experiment for isolated loadings, particularly when they are represented as point forces in a theoretical analysis. In the panel studied and in other similar cases there will always be ample structural material to further partition the model. This partitioning of a structure permits the desirable attenuation of the effect of load concentrations. These load concentrations can create discrepancies between computational and experimental results.

In an associated study, the wing center section is being included in the over-all wing analysis. The inclusion of the energy contribution from the center section would not be expected to change the theoretical analysis in the vicinity of the particular panel considered in this report. This is because of the massive construction of the wing in this specific area. Even though the pivot rib is not infinitely rigid in the chordwise direction, it is nearly so and may be assumed to have zero flexibility. Reference 3 verifies this assumption by the close agreement between the theoretical and experimental results in the vicinity of the particular panel considered.

CHAPTER VII

CONCLUSIONS AND RECOMMENDATIONS

Conclusions

It can therefore be concluded that a valid comparison was achieved between theoretical and experimental strain energies of a thick milled skin aircraft structure. The accuracy of the analytical method is subject to the absence of concentrated loadings. Additionally, for a theoretical structure, a fine element partitioning procedure is required.

The analytical method provided remarkably accurate results (2.94 per cent error) and is a valid approach to aircraft structures of this specific type.

Recommendations

It is recommended that even though the results of this study are favorable, another analysis should be made on a panel that is subjected to more severe non-planar loadings. Possibly a panel outboard of the intermediate rib could be used on the same wing. The load would then be applied to a thinner section of the wing where there is less torsional rigidity, and the point of load application would be closer to the panel to be studied. Another possibility would be to obtain some means of applying single point loads to the same panel at the intersection of the intermediate rib and the spanwise beams. Still another method would be to apply

the same torque used in this analysis at the intermediate rib.

An additional recommendation, that was previously discussed in Chapter III, is that a study be conducted to determine the validity of a wing analysis that neglects the presence of any rib flanges.

REFERENCES

1. Peery, David J., Aircraft Structures, McGraw-Hill Book Company, New York, 1950.
2. Argyris, J. H. and Kelsey, S., Energy Theorems and Structural Analysis, Butterworths, London, 1960.
3. Holgren, Marvin A. and Comfort, Clayton L., Comparison of Experimental Stresses and Deflections with Those Predicted by a Strain Energy Method for an F8U-3 Wing Loaded in Torsion, MS Thesis, Naval Postgraduate School, 1963.
4. Smith, F. C., Stress and Deflection Analysis of Aircraft Structures Using Strain Energy Theory in Conjunction with Electronic Digital Computers, Chance Vought Aircraft Incorporated, Dallas, Texas, 1957.
5. Bilodeau, J. W., F8U-3 Structural Description Report, Chance Vought Aircraft Incorporated, Dallas, Texas, 1957.
6. Garvey, S. J., "The Quadrilateral Shear Panel," Aircraft Engineering, May, 1951.
7. Wang, Chi-Teh, Applied Elasticity, McGraw-Hill Book Company, New York, 1953.
8. Grzedzielski, A. L. M., Theory of Multi-Spar and Multi-Rib Wing Structures, National Aeronautical Establishment, Ottawa, Canada, 1961.

9. Bruhn, E F., Analysis and Design of Flight Vehicles Structures, Tri-State Offset Company, Cincinnati, Ohio, 1965.

10. Kane, D. A., Wing Stress Analysis, Chance Vought Aircraft Incorporated, Dallas, Texas, 1958.

11. Gallagher, Richard H., A Correlation Study of Methods of Matrix Structural Analysis, The MacMillan Company, New York, 1964.

12. Eggwertz, Sigge, Calculation of Stresses in a Swept Multicell Cantilever Box Beam with Ribs Perpendicular to the Spars and Comparison with Test Results, The Aeronautical Research Institute of Sweden, Stockholm, 1954.

APPENDIX A

THEORETICAL DETERMINATION OF SHEAR FLOWS AT SECTIONS PERPENDICULAR TO CIB AT $y_w = 98.7$ and $y_w = 74.3$ (Reference 3)

The theoretical shear flows at sections perpendicular to the CIB at $y_w = 98.70$ and $y_w = 74.30$ were calculated in order to determine the shear flows at both sections which would be used to produce the equivalent applied forces at the streamwise intermediate rib, $y_w = 81.98$. The cross-sections are shown schematically in Figure A1. The thicknesses were averaged mid-panel values, and the web heights were taken as the mid-panel height between the upper and lower skins.

A box structure with several cells will have one less redundant than the number of cells. In this case, there are five redundant webs. It is desired to write six equations in six unknown shear flows. This was done by equating the angle of twist of one cell with the remaining five, which gives five equations, and then writing an equilibrium of torsional moments equation.

The first five equations were obtained by equating the angle of twist per unit length, Θ, of one cell with the other five using the well-known expression for a box beam,

$$\Theta = \sum \frac{q \Delta s L}{2 A_t G} \qquad \text{(A1)}$$

FIG. A1

SCHEMATIC DIAGRAM OF SECTIONS PERPENDICULAR TO THE C.I.B. AT y_w = 98.7 AND 74.3

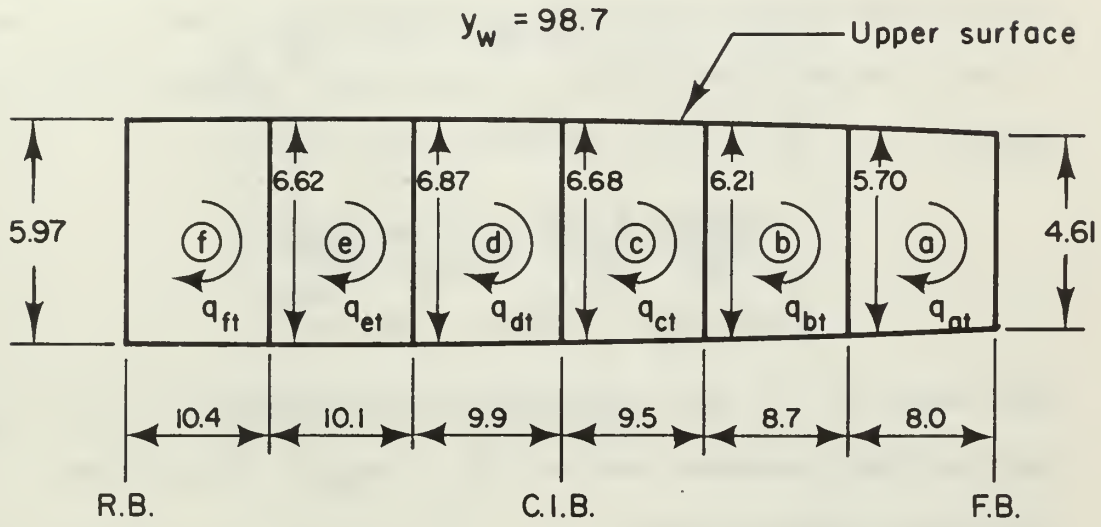

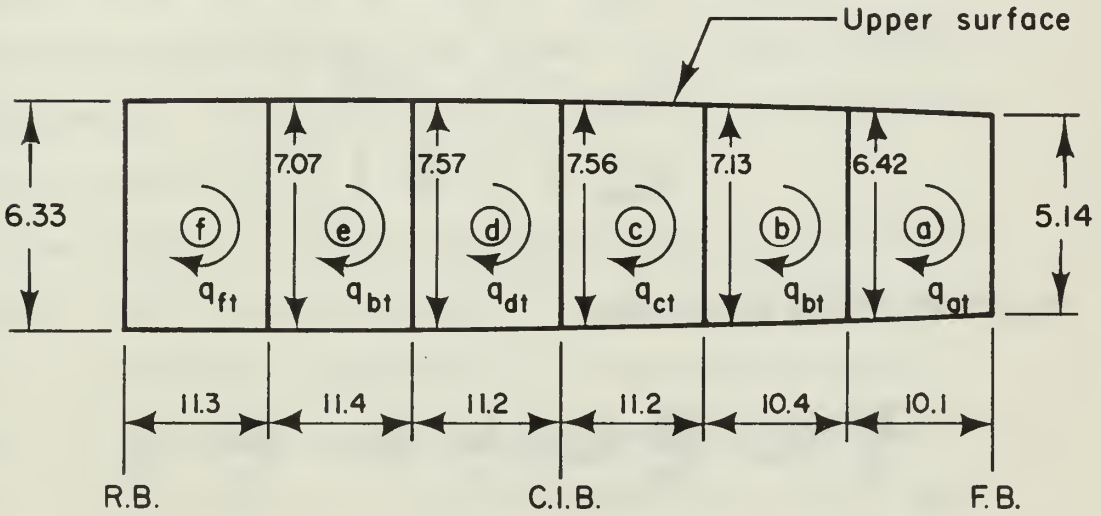

y_w = 74.3

Note: dimensions in inches (ref. 10)

The equilibrium of torsional moments may be written as

$$T = \sum 2 A_n q_n \tag{A2}$$

In using Equation A2 the summation is carried out around the entire perimeter of each cell. The unit length, L, and the constant factor 2G drop out, leaving for cells a and b,

$$\sum_a \frac{q \Delta s}{A_{at}} = \sum_b \frac{q \Delta s}{A_{bt}} \tag{A3}$$

The value of q for any exterior web of cell a is q_{at} and for the interior web is $(q_{at} - q_{bt})$. Using the following abbreviations,

$$\delta_{aa} = \sum_a \frac{\Delta s}{t}$$

$$\delta_{bb} = \sum_b \frac{\Delta s}{t}$$

$$\delta_{ab} = \left[\frac{\Delta s}{t} \right]_{a--b}$$

Equation A3 is rewritten,

$$\frac{q_{at}}{A_a} \delta_{aa} - \frac{q_{bt}}{A_a} \delta_{ab} = \frac{q_{bt}}{A_b} \delta_{bb} - \frac{q_{at}}{A_b} \delta_{ab} \tag{A4}$$

The terms δ_{aa} and δ_{bb} represent summations around the entire perimeter of their respective cells and δ_{ab} the value for the interior web. The enclosed areas were taken as the average web height times the distance between webs.

Equating the angle of twist per unit length of cell a to the remaining cells yields the following equations:

$$\frac{1}{A_a}(q_{at}\delta_{aa} - q_{bt}\delta_{ab}) =$$

$$= \frac{1}{A_b}(q_{bt}\delta_{bb} - q_{at}\delta_{ab} - q_{ct}\delta_{bc})$$
$$= \frac{1}{A_c}(q_{ct}\delta_{cc} - q_{bt}\delta_{bc} - q_{dt}\delta_{cd})$$
$$= \frac{1}{A_d}(q_{dt}\delta_{dd} - q_{ct}\delta_{cd} - q_{et}\delta_{de})$$
$$= \frac{1}{A_e}(q_{et}\delta_{ee} - q_{dt}\delta_{de} - q_{ft}\delta_{ef})$$
$$= \frac{1}{A_f}(q_{ft}\delta_{ff} - q_{et}\delta_{ef})$$

Making appropriate substitutions, performing the indicated algebraic operations and rearranging, one obtains five equations in terms of the six shear flows with constant coefficients. The required sixth equation was derived as previously described.

The solution to these six simultaneous equations was obtained from a digital computer using a FORTRAN program which is included in Reference 3. It utilizes Gauss's method of elimination with row pivoting and back substitution and is designed to yield solutions for one or more column vectors forming the right hand side of the set of equations. This means that it would produce solutions for one or more values of applied torque. The check values of q were hand calculated using an iterative procedure

suggested by Bruhn in Reference 9 and within slide rule accuracy agree well with the computer solutions.

APPENDIX B
CALIBRATION CURVES FOR DILLON DYNAMOMETERS AND HYDRAULIC PRESSURE SYSTEM

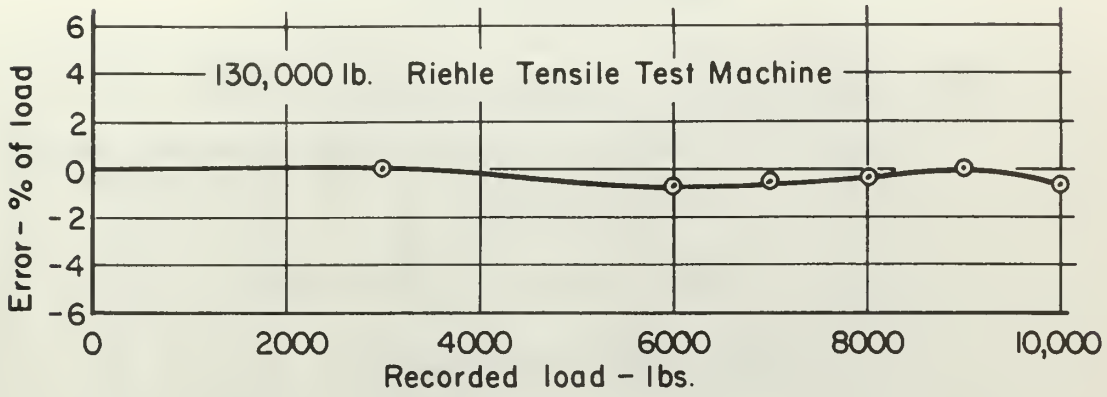

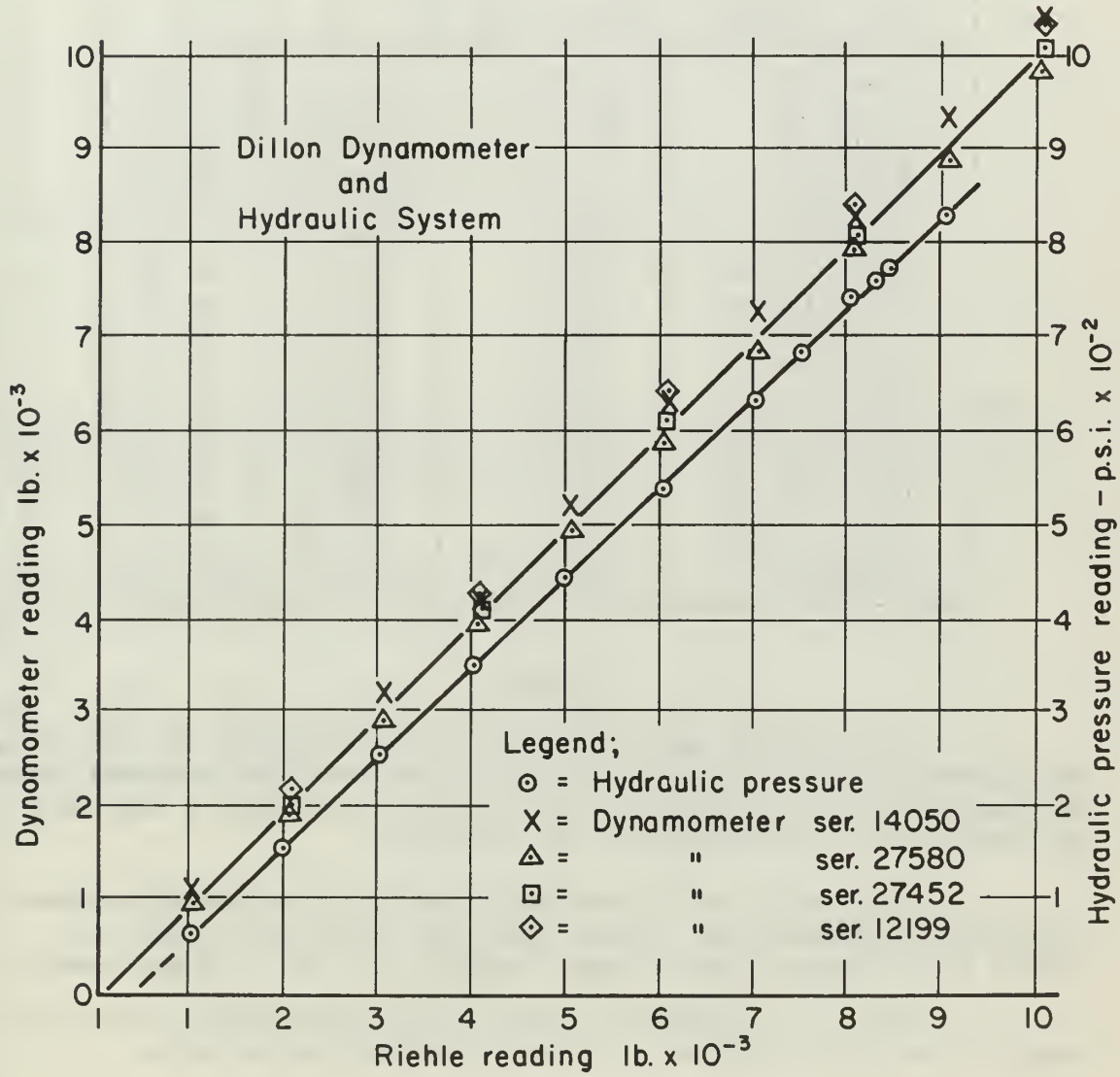

APPENDIX C

CO-ORDINATE LOCATION OF STRAIN GAGES

F8U-3 WING PANEL

Note: Co-ordinate origins are as follows:

$x_w = 0$ = Intersection of center section droop leading edge and the center line of the aircraft.

$y_w = 0$ = The aircraft center line.

UPPER SKIN INSIDE GAGES

Gage Number	Gage Type	x_w	y_w
83-84-85	AR-7-2	137.72	28.53
86-87-88	AR-7-2	140.00	32.25
89-90-91	AR-7-2	142.55	30.48
92-93-94	AR-7-2	145.25	28.74
95-96-97	AR-7-2	147.99	45.40
98-99-100	AR-7-2	150.30	43.84
101-102-103	AR-7-2	152.73	42.25
104-105-106	AR-7-2	155.95	58.68
107-108-109	AR-7-2	158.11	57.21
110-111-112	AR-7-2	160.24	55.74
113-114-115	AR-7-2	163.84	71.68
116-117-118	AR-7-2	165.77	70.51
119-120-121	AR-7-2	167.72	69.19
122-123-124	AR-7-2	169.23	78.83
125-126-127	AR-7-2	170.60	78.83
128-129-130	AR-7-2	173.00	78.83
40-41-42	AR-7-2	168.56	75.10

NOTES

1. All strain gage rosettes were mounted at the Naval Postgraduate School and oriented with one leg perpendicular to the CIB, the 45 degree gage pointing outboard and aft, and the third leg parallel to the CIB.

2. All gages were manufactured by the Baldwin-Lima-Hamilton Corporation, taken from lot B-31 and rated at 120.5 $\pm$ 0.5 ohms with a gage factor of 1.97 $\pm$ 2 per cent.

3. The low numbered rosette leg identifies the gage and is the leg parallel to the Load Reference Axis.

4. Gage No. 98 yields questionable results.

UPPER SKIN OUTSIDE GAGES

Gage Number	Gage Type	x_w	y_w
580-581-582	AR-7-2	137.72	28.53
583-584-585	AR-7-2	140.00	32.25
475-476-477	AR-7-2	142.55	30.48
586-587-588	AR-7-2	145.25	28.74
589-590-591	AR-7-2	147.99	45.40
592-593-594	AR-7-2	150.30	43.84
595-596-597	AR-7-2	152.73	42.25
598-599-600	AR-7-2	155-95	58.68
601-602-603	AR-7-2	158.11	57.21
604-605-606	AR-7-2	160.24	55.74
607-608-609	AR-7-2	163.84	71.68
610-611-612	AR-7-2	165.77	70.51
613-614-615	AR-7-2	167.72	69.19
616-617-618	AR-7-2	169.23	78.83
619-620-621	AR-7-2	170.60	78.83
622-623-624	AR-7-2	173.00	78.83
625-626-627	AR-7-2	168.56	75.10

NOTES

1. All strain gage rosettes were mounted at the Naval Postgraduate School and oriented with one leg perpendicular to the CIB, the 45 degree gage pointing outboard and aft, and the third leg parallel to the CIB.

2. All gages were manufactured by the Baldwin-Lima-Hamilton Corporation, taken from lot B-31 and rated at 120.5 $\pm$ 0.5 ohms with a gage factor of 1.97 $\pm$ 2 per cent.

3. The high numbered rosette leg identifies the gage and is the leg parallel to the Load Reference Axis.

APPENDIX D

STRAIN GAGE INSTRUMENTATION

The method of taking strain readings employed common Wheatstone Bridge circuitry as is shown in Figure D1. The experimental test setup used the Budd/Datran Digital Strain Indicator (Model TC22). The Wheatstone Bridge and all associated circuits were incorporated within the indicator. The indicator interpreted the bridge unbalance and gave a visual display of the strain directly in units of micro-inches per inch.

When the test runs were made, each of the twenty gages connected through the switching and balancing unit was zeroed on the digital strain indicator in the conventional manner prior to load application. At any time during the test run the calibration could be checked by merely pushing a button on the counter. This gave a continual check and ensured the calibration of the counter at all times during the running of the test.

FIG. D1
SCHEMATIC DIAGRAM
STRAIN GAGE INSTRUMENTATION

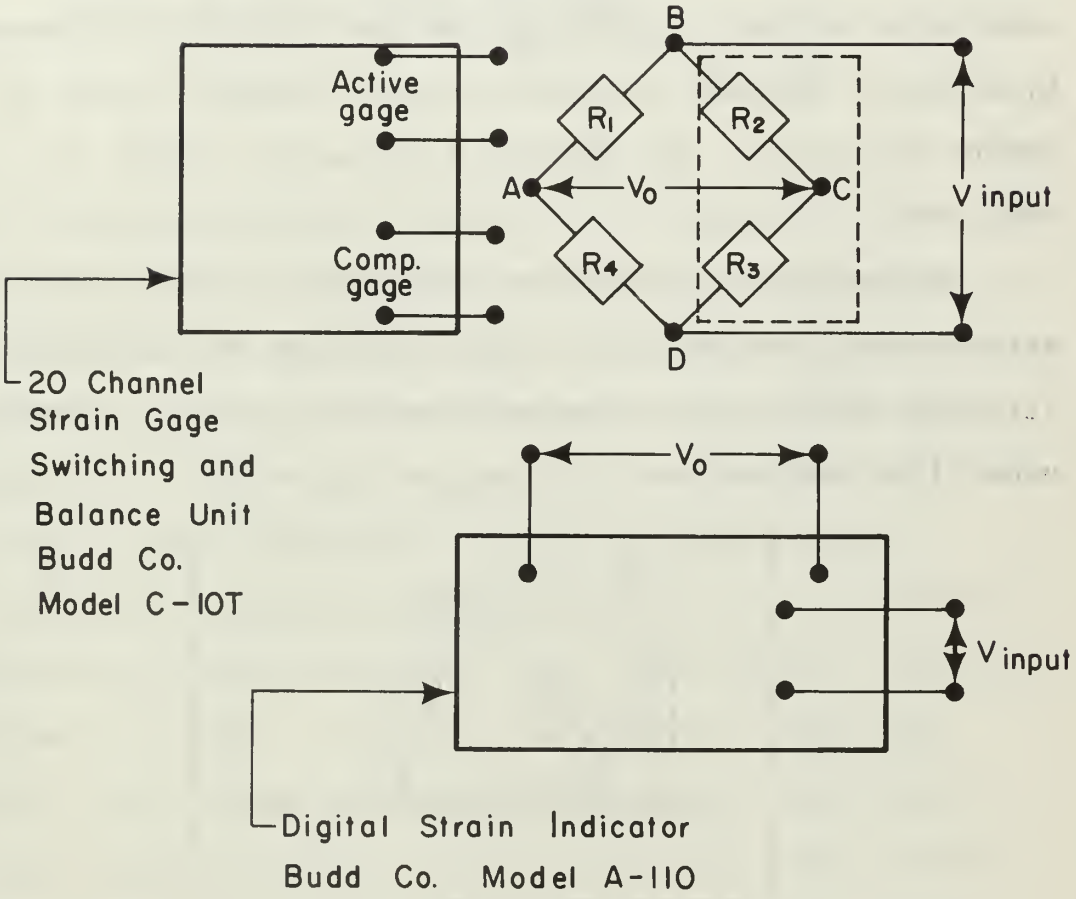

$R_1 = R_4$ = 120.5 ohms

$R_2 = R_3$ = 120.5 ohms

Resistance tolerance: 5%

Linearity tolerance: 0.5%

APPENDIX E

EXPERIMENTAL PRINCIPAL STRESSES AND AXIS ORIENTATION

The magnitudes of the principal stresses, maximum shear stresses and orientations were calculated for each rosette on both sides of the wing panel. The experimental strain gage readings are tabulated in Table EI. Calculations were simplified through the use of the IBM 360 Digital Computer utilizing a FORTRAN IV program named "RECROSE" shown in Tables E2 and E3. The RECROSE results are listed in Table E4.

The program was designed around the standard relationship between rectangular rosette readings and principal stresses found in any standard text (e.g., Wang in Reference 7) on the subject.

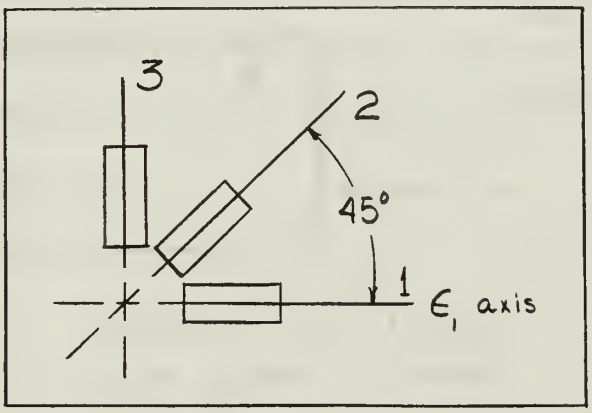

Figure E1

$$\sigma_{max} = \frac{E}{2}\left[\frac{\epsilon_1+\epsilon_2}{(1-\mu)} + \frac{1}{(1+\mu)}\sqrt{(\epsilon_1-\epsilon_3)^2+\left[2\epsilon_2-(\epsilon_1+\epsilon_3)\right]^2}\right]$$

$$\sigma_{min} = \frac{E}{2}\left[\frac{\epsilon_1+\epsilon_3}{(1-\mu)} - \frac{1}{(1+\mu)}\sqrt{(\epsilon_1-\epsilon_3)^2 + \left[2\epsilon_2-(\epsilon_1+\epsilon_3)\right]^2}\right]$$

$$\sigma_{max} = \frac{E}{2(1+\mu)}\sqrt{(\epsilon_1-\epsilon_3)^2 + \left[2\epsilon_2-(\epsilon_1+\epsilon_3)\right]^2}$$

$$\phi_p = \frac{1}{2}\arctan\left[\frac{2\epsilon_2-(\epsilon_1+\epsilon_3)}{\epsilon_1+\epsilon_3}\right]$$

ϕ_p is the angle between leg number one and the maximum normal stress axis. A positive value indicates an angle in the direction of ϵ_2. ϵ_1, ϵ_2 and ϵ_3 are the strain gage readings on their respective legs shown in Figure E1. The number of the rosette leg parallel to the Load Reference Axis (CIB) is the identifying number for the rosette.

The input to program RECROSE (Table EI) was designed to accommodate the above notation. Only the rosette identifying number is listed. This is also the gage number for which the first column of strains is listed. The second and third columns are then the values of the strain on the next two consecutive numbered gages comprising the rosette.

This program was designed for 7079-T6 Aluminum with a Modulus of Elasticity of 10.3×10^6 pounds per square inch and a Poisson's ratio of 0.32.

The results of RECROSE are listed in Table E4 and are identified by the rosette numbers which orient the reference axis for ϕ_p.

TABLE EI

EXPERIMENTAL STRAIN READINGS

(Input to RECROSE Program)

336,000 in. lb. load

Rosette Number	ϵ_1 μ in./in.	ϵ_2 μ in./in	ϵ_3 μ in./in.
INSIDE SKIN			
83	9	51	-12
86	12	59	-10
89	15	55	-20
92	13	52	-21
95	12	83	-3
98	19	83	-8
101	20	91	-4
104	18	109	-7
107	10	110	-6
110	21	107	-12
113	14	136	-2
116	17	136	-13
119	22	130	-16
122	20	147	-11
125	12	152	-15
128	17	151	-21
40	26	149	-19
OUTSIDE SKIN			
582	10	59	-18
585	12	70	-13
477	18	65	-20
588	26	69	-26
591	22	87	-20
594	32	92	-26
597	26	89	-26
600	20	124	-12
603	25	123	-16
606	30	120	-18
609	20	152	-23
612	29	154	-14
615	22	146	-6
618	32	169	-19
621	32	169	-30
624	33	177	-13
627	33	167	-23

TABLE E2

LIST OF SYMBOLS USED IN

PROGRAM RECROSE

Computer Coded Name	Definition
E1	ϵ_1, strain in identifying leg of rosette.
E2	ϵ_2, strain in diagonal leg of rosette.
E3	ϵ_3, strain in perpendicular leg of rosette.
SIGMAX	σ_{max}, maximum principal stress.
SIGMIN	σ_{min}, minimum principal stress.
SIGMA 1	σ_1, stress in identifying leg of rosette.
SIGMA 3	σ_3, stress in perpendicular leg of rosette.
TAUMAX	τ_{max}, maximum shearing stress.
PHIPRR	ϕ_p, angle from ϵ_1 to σ_{max} axis.
N	The number of input rosettes.
E	Modulus of Elasticity.
U	μ, Poisson's ratio.

TABLE E3

FORTRAN IV PROGRAM

"RECROSE"

```
//RECROSE JOB  2802 , PARCELLS ,MSGLEVEL 0                                      0001
// EXEC FORTCLG                                                                 0002
//FORT.SYSIN DD *                                                               0003
C      RECTANGULAR STRAIN ROSETTE DATA REDUCTION FOR THE DETERMINATION         C004
C      OF PRINCIPAL AXES, PRINCIPAL STRESSES, MAXIMUM SHEARING STRESSES,       0005
C      AND STRESSES ALONG THE ROSETTE AXES 1 AND 3.                            0006
C                                                                              C007
C                                                                              0008
       READ  5,100  N,E,U                                                      0009
       L 0                                                                     001C
       I 0                                                                     0011
     1 I I 1                                                                   0012
       READ  5,101  IGAGE,E1,E2,E3                                             0013
       E1 E1*1.0E-06                                                           C014
       E2 E2*1.0E-06                                                           0015
       E3 E3*1.0E-06                                                           0016
C      CORRECTION FOR A GAGE FACTOR   1.95                                    1GFC
       E1 E1*1.03                                                             2GFC
       E2 E2*1.03                                                             3GFC
       E3 E3*1.03                                                             4GFC
       G 1.0-U                                                                 0017
       H 1.0 U                                                                 0018
       A E1 E3                                                                 0019
       B E1-E3                                                                 0020
       C  2.0*E2 -A                                                            0021
       R SQRT  B**2   C**2                                                     0022
       TAUMAX  E/ 2.0*H  *R                                                    0023
       SIGMAX  E/2.0 *  A/G   R/H                                              0024
       SIGMIN  E/2.0 *  A/G - R/H                                              0025
       PHIPRR 0.5* ATAN2 C,B                                                   0026
       IF  B.GE.0.0  GO TO 2                                                   0027
       PHIPRR PHIPRR 1.5707963                                                 0028
     2 PHIPRD PHIPRR/.1745329E-01                                              0029
       D TAUMAX*COS 2.0*PHIPRR                                                 0030
       SIGMA1   SIGMAX SIGMIN /2.0  D                                          0031
       SIGMA3   SIGMAX SIGMIN /2.0 -D                                          0032
       TAUO -TAUMAX*SIN 2.0*PHIPRR                                             0033
       IF  I.GT.1  GO TO 3                                                     0034
       WRITE  6,102                                                            0035
     3 WRITE  6,103  IGAGE,E1,SIGMAX,E2,SIGMIN,E3,TAUMAX,SIGMA1,PHIPRR,       0036
      9SIGMA3,PHIPRD,TAUO                                                      0037
       L L 11                                                                  0038
       IF  L.LT.66  GO TO 4                                                    0039
       WRITE  6,102                                                            004C
       L 0                                                                     0041
     4 IF  I.LT.N  GO TO 1                                                     0042
   10C FORMAT  I8,E17.7,F10.5                                                  0043
   101 FORMAT  I8,3F12.5                                                       0044
   102 FORMAT  1H1                                                             0045
   103 FORMAT  T6, ROSETTE NUMBER ,I8,//,T16, E1  ,F14.7,  IN/IN ,T45,         0046
      3 SIGMAX  ,F14.7,  PSI ,/,T16, E2  ,F14.7,  IN/IN ,T45, SIGMIN  ,       0047
      3F14.7,  PSI ,/,T16, E3  ,F14.7,  IN/IN ,T45, TAUMAX  ,F14.7,           0048
      3  PSI ,//,T11, SIGMA 1  ,F14.7,  PSI ,T45, PHI PR  ,F14.7,  RADIAN    0049
      3S ,/,T11, SIGMA 3  ,F14.7,  PSI ,T45, PHI PR  ,F14.7,  DEGREES ,/,     C050
      3T13, TAU O  ,F14.7,  PSI ,//                                           0051
       RETURN                                                                 0052
       END                                                                    C053
```

TABLE E4

EXPERIMENTAL RESULTS

(Output of Program RECROSE)

Rosette	SIGMA 1	SIGMA 3	SIGMAX	SIGMIN	TAUMAX	PHIPRR
83	60.987	-107.792	406.902	-453.706	430.304	39.345
86	104.009	-72.807	490.063	-458.860	474.462	39.630
89	101.646	-179.653	444.059	-522.066	483.063	36.536
92	74.225	-199.037	407.954	-532.765	470.359	36.556
95	130.485	9.928	703.993	-563.579	633.786	42.271
98	194.309	-22.693	718.064	-546.448	632.256	40.059
101	221.257	28.366	798.828	-549.205	674.016	40.886
104	186.273	-14.657	923.694	-752.078	837.886	41.556
107	95.500	-33.094	901.589	-839.184	870.386	42.881
110	202.819	-62.407	904.616	-764.203	834.409	40.427
113	157.906	29.310	1140.408	-953.191	1046.799	43.239
116	151.760	-89.355	1114.900	-1052.495	1083.697	41.806
119	199.510	-105.901	1078.876	-985.268	1032.072	40.745
122	194.782	-54.369	1222.249	-1081.836	1152.042	41.896
125	85.100	-131.904	1215.054	-1261.858	1238.457	42.487
128	121.503	-183.908	1207.919	-1270.324	1239.123	41.461
40	235.441	-126.231	1237.903	-1128.693	1183.298	40.605
582	50.114	-174.925	456.284	-581.095	518.689	38.736
585	92.664	-108.265	567.653	-583.255	575.454	39.973
477	137.104	-168.307	536.391	-567.594	551.992	36.970
588	208.965	-208.965	592.624	-592.624	592.624	34.646
591	184.381	-153.178	727.102	-695.899	711.500	38.139
594	279.881	-186.272	799.123	-705.514	752.318	35.976
597	208.965	-208.965	745.201	-745.201	745.202	36.857
600	191.000	-66.189	1035.393	-910.581	972.987	41.203
603	234.968	-94.555	1036.749	-896.336	966.543	40.093
606	286.500	-99.282	1029.923	-842.706	936.314	39.056
609	149.397	-196.200	1222.335	-1269.139	1245.737	41.013
612	289.809	-55.787	1307.058	-1073.037	1190.048	40.825
615	237.332	12.291	1239.625	-990.002	1114.814	42.104
618	306.356	-103.538	1423.420	-1220.602	1322.012	40.541
621	264.754	-233.550	1388.629	-1357.425	1373.029	39.772
624	340.868	-28.840	1510.879	-1198.849	1354.865	41.079
627	303.047	-147.033	1399.322	-1243.308	1321.316	40.097

INITIAL DISTRIBUTION LIST

		No. Copies
1.	Defense Documentation Center Cameron Station Alexandria, Virginia 22314	20
2.	Library Naval Postgraduate School Monterey, California 93940	2
3.	Professor Charles H. Kahr Department of Aeronautics Naval Postgraduate School Monterey, California 93940	2
4.	Lieutenant Paul W. Parcells 1221 Spruance Road Monterey, California 93940	1
5.	Commander, Naval Air Systems Command Department of the Navy Washington, D. C. 20360	1
6.	Chairman, Department of Aeronautics Naval Postgraduate School Monterey, California 93940	1
7.	Professor Allen E. Fuhs Department of Aeronautics Naval Postgraduate School Monterey, California 93940	1
8.	Professor Ulrich Haupt Department of Aeronautics Naval Postgraduate School Monterey, California 93940	1
9.	Professor Robert E. Ball Department of Aeronautics Naval Postgraduate School Monterey, California 93940	1
10.	Dr. E. S. Lamar Chief Scientist Naval Air Systems Command Department of Navy Washington, D. C. 20360	1

11. Mr. G. L. Desmond 1
Aerodynamics and Structures
Technology Administrator
Naval Air Systems Command
Department of Navy
Washington, D. C. 20360

DOCUMENT CONTROL DATA - R&D

(Security classification of title, body of abstract and indexing annotation must be entered when the overall report is classified)

1. ORIGINATING ACTIVITY *(Corporate author)*
Naval Postgraduate School
Monterey, California

2a. REPORT SECURITY CLASSIFICATION
Unclassified

2b. GROUP

3. REPORT TITLE
Theoretical and Empirical Analyses of Thick Skinned Swept Wing Panels

4. DESCRIPTIVE NOTES *(Type of report and inclusive dates)*
Masters Thesis 1967-1968

5. AUTHOR(S) *(Last name, first name, initial)*
PARCELLS, Paul W., LT, USN

6. REPORT DATE	7a. TOTAL NO. OF PAGES	7b. NO. OF REFS
December 1967	71	12

8a. CONTRACT OR GRANT NO.

b. PROJECT NO.

c.

d.

9a. ORIGINATOR'S REPORT NUMBER(S)

9b. OTHER REPORT NO(S) *(Any other numbers that may be assigned this report)*

10. AVAILABILITY/LIMITATION NOTICES
[redacted]

11. SUPPLEMENTARY NOTES

12. SPONSORING MILITARY ACTIVITY
Commander, Naval Air Systems Command
Department of the Navy
Washington, D. C. 20360

13. ABSTRACT

The validity of conventional skin and stringer type analyses is verified experimentally for a thick milled skin aircraft structure. The accuracy of solution is evaluated by comparing the strain energies in a mathematical model to that obtained experimentally from a wing panel of a high performance aircraft.

Results indicate that the conventional methods of a skin-stringer/matrix force approach are valid for a thick milled skin aircraft structure of this type provided the panel loading is neither severe nor concentrated. Additionally the grid elements chosen must be small enough to preclude any gross averaging errors.

DD FORM 1 JAN 64 1473

14. KEY WORDS	LINK A		LINK B		LINK C	
	ROLE	WT	ROLE	WT	ROLE	WT
SWEPT WING						
THICK MILLED SKIN						
MATRIX FORCE METHOD						